Original Research (Basic)

Differential Expression of Alkaline Phosphatase and PHOSPHO1 in Bone from a Murine Model of Chronic Kidney Disease

Shun-Neng Hsu[1, 2], Louise A Stephen[1], Scott Dillon[1], Elspeth Milne[1], Amanda Novak[1], Jose Luis Millán[3], Vicky E Macrae[1], Katherine A Staines[4], and Colin Farquharson[1]

[1]The Roslin Institute and Royal (Dick) School of Veterinary Studies, University of Edinburgh, Easter Bush, Midlothian, UK

[2]Division of Nephrology, Department of Medicine, Tri-Service General Hospital, National Defense Medical Center, Taipei, Taiwan

[3] Sanford Burnham Prebys Medical Discovery Institute, La Jolla, USA.

[4]School of Pharmacy and Biomolecular Sci, University of Brighton, Brighton, UK

RUNNING TITLE: Bone mineralization in chronic kidney disease

CORRESPONDENCE:

Shun-Neng Hsu, M.D.

The Roslin Institute and Royal (Dick) School of Veterinary Studies, University of Edinburgh, Easter Bush, Midlothian, EH25 9RG, UK

Tel: +44 (0)131 651 9156

Email: s1734748@sms.ed.ac.uk

ABSTRACT

Chronic kidney disease-mineral bone disorder (CKD-MBD) is a systemic disorder characterized by altered mineral and bone metabolism. The role of PHOSPHO1 and tissue-nonspecific alkaline phosphatase (TNAP) in controlling bone mineralization in CKD-MBD is unclear. We utilized the adenine-induced murine model of CKD-MBD in which mice present with hyperphosphatemia, hyperparathyroidism, and elevated FGF23 levels, and bone turnover markers. Micro-CT and histomorphometric analysis revealed microarchitectural changes to the trabecular and cortical bone of CKD mice. Furthermore, CKD cortical bone mineral density (BMD) was increased ($p < 0.05$) whereas CKD trabecular bone BMD was decreased ($p < 0.05$). These changes were accompanied by decreased *Alpl* mRNA expression ($p < 0.001$) and increased *Phospho1* mRNA expression ($p < 0.01$) in CKD bones, which were confirmed at the protein level. Cortical bone BMD was unchanged in *Phospho1* knockout (P1KO) CKD mice suggesting that the increased cortical BMD noted in CKD was driven by the increased PHOSPHO1 expression. Intriguingly, other structural parameters were improved in P1KO CKD mice. In an attempt to determine the causes of the mineralization defects noted in the CKD mice, we investigated the direct effects of FGF23, PTH, and phosphate (Pi) administration on PHOSPHO1 and TNAP expression by primary murine osteoblasts. PHOSPHO1 and TNAP expression were down-regulated in a concentration-dependent manner by Pi and PTH whereas the effects of FGF23 treatment, with or without klotho, were less marked. Osteoblast matrix mineralization was increased with Pi, decreased with PTH in a concentration-dependent manner and FGF23 had no effect. In summary, this pre-clinical model of CKD presented with hypomineralization of trabecular bone but hypermineralisation of cortical bone. Similarly, divergent expression levels of TNAP and PHOSPHO1 were noted in CKD. These novel observations implicate these key phosphatases in the etiology of CKD-MBD and may help explain the disordered skeletal mineralization characteristic of this progressive disorder.

KEY WORDS: Bone mineralization; chronic kidney disease (CKD); chronic kidney disease–mineral and bone disorder (CKD-MBD); PHOSPHO1; tissue-nonspecific alkaline phosphatase (TNAP)

Introduction

Chronic kidney disease (CKD) is an irreversible and progressive disorder characterized by a

gradual loss of kidney function over time [1]. Patients with advanced CKD frequently develop disturbances of mineral and bone metabolism and fail to maintain normal systemic levels of calcium (Ca), inorganic phosphate (Pi), parathyroid hormone (PTH), and fibroblastic growth factor-23 (FGF23) [2,3]. Systemic abnormalities (hyperphosphatemia, hyperparathyroidism, and elevated FGF-23) are the primary indicators for the diagnosis of CKD–mineral bone disorder (CKD–MBD) which develops in the early stages of CKD and disease progression can eventually result in bone fractures as well as vascular calcification [4]. The current classification system and treatment strategy for bone disorders in CKD-MBD are based on the assessment of three key histologic descriptors - changes in bone turnover (T), mineralization (M), and volume (V) (TMV system) [5,6]. The bone mineralization defect is particularly common in patients with late-stage CKD-MBD and this, and the other CKD-associated skeletal pathologies, have been attributed to CKD-related metabolic and hormonal disturbances [7,8].

Although the precise mechanisms responsible for the impaired skeletal mineralization observed in CKD-MBD remain unclear, the origins are likely to involve a complex interplay between bone and the altered endocrine milieu. Phosphorus retention, due to the failing kidney, leads to chronically elevated concentrations of circulating FGF23 in an attempt to normalize serum Pi levels through enhanced urinary secretion and decreased intestinal absorption [9]. This is achieved by the inhibition of renal 1α-hydroxylase and stimulation of 24-hydroxylase but the resulting reduction in circulating levels of 1, 25$(OH)_2D_3$ contributes to hypocalcemia and the development of secondary hyperparathyroidism (SHPT) [10,11]. The SHPT, which is particularly prevalent in advanced CKD stages, promotes bone resorption by increasing the receptor activator of nuclear factor-□B ligand (RANKL)/osteoprotegerin (OPG) ratio [12,13]. The bone formed during rapid remodeling is both immature and poorly mineralized [14]. It is also possible however that altered endocrine factors may directly target the expression of key phosphatases critical for skeletal mineralization. Specifically, FGF23 may inhibit matrix mineralization by suppressing tissue-nonspecific alkaline phosphatase (TNAP) expression and activity by osteoblasts [15-17] and PTH may induce a rapid downregulation of *Phospho1* gene expression in osteogenic cells and bone marrow stromal cell lines [18-20].

PHOSPHO1 and TNAP are two of the most widely studied phosphatases involved in skeletal mineralization [21,22]. PHOSPHO1 is expressed at sites of mineralization such as in the

hypertrophic zone of the growth plate and bone-forming surfaces of both long bones and calvaria [23,24]. During mineralization, PHOSPHO1 liberates Pi to be incorporated into the mineral phase through hydrolysis of its substrates phosphocholine (PCho) and phosphoethanolamine (PEA) leading to an increase in the phosphate/inorganic pyrophosphate (Pi/PPi) ratio within matrix vesicles [25]. *Phospho1* deficient mice exhibit defects in bone mineralization, decreased bone mineral density (BMD), compromised trabecular and cortical bone microarchitecture, and spontaneous greenstick fractures [26,27]. TNAP is an ectoenzyme and is highly expressed on the membranes of osteoblasts, chondrocytes, and matrix vesicles [28,29]. It hydrolyzes PPi, a potent extracellular inhibitor of mineralization to allow the propagation of hydroxyapatite in the extracellular matrix (ECM), beyond the confines of the matrix vesicle membrane [30]. Mice deficient in TNAP function ($Alpl^{-/-}$) phenocopy infantile hypophosphatasia (HPP), an inborn error of metabolism resulting in rickets and osteomalacia [31]. A complete absence of ECM mineralization is observed in $Phospho1^{-/-}$; $Alpl^{-/-}$ double knockout mice and in murine metatarsals cultured in the presence of PHOSPHO1 and TNAP inhibitors demonstrating the requirement and functional co-operativity of PHOSPHO1 and TNAP for bone mineralization [32,33].

Despite great advances being made in understanding the mechanisms responsible for the compromised bone mineralization noted in CKD-MBD, the involvement of phosphatases has not been studied. Therefore, in this study, we examined the expression of PHOSPHO1 and TNAP in long bones of a murine model of CKD-MBD and further examined the effects of PTH, FGF23, and Pi on TNAP and PHOSPHO1 expression in murine calvarial osteoblasts. Such information provides insight into the mechanisms responsible for the altered skeletal mineralization in CKD-MBD.

Materials and Methods

Mice

C57BL/6 male mice were purchased from Charles River Laboratories (Currie, UK) and were used in our first *in vivo* CKD-MBD study. Male *Phospho1* knockout (P1KO) mice and littermate wild-type (WT) controls, maintained on a C57BL/6 background were generated as previously described [32] and used in our second *in vivo* CKD-MBD study. Offspring carrying the mutant *Phospho1* gene were identified by genotyping using PCR (F: 5′-TCCTCCTCACCTTCGACTTC-3′, R: 5′-TCCTCCTCACCTTCGACTTC-3′). All mice were maintained under standard housing conditions with a 12-hour light-dark cycle and with

access to food and water until 8-weeks of age at which point, they were randomly assigned a control (CTL; n = 12) or CKD (n = 12) diet and maintained on their respective diets for 5 weeks (Fig. 1A). Body weights (BW) were recorded twice weekly to monitor health conditions until the third week of study and then daily till sacrifice. Mice losing more than 30% of their BW compared to mice of the control group or reaching the threshold, listed in the scoring sheet were euthanized by exposure to CO_2 and confirmed dead by cervical dislocation. All animal experiments were approved by the Roslin Institute's named veterinary surgeon and named animal care and welfare officer (NACWO), with animals maintained in accordance with the Home Office code of practice (for the housing and care of animals bred, supplied, ARRIVE guidelines or used for scientific purposes).

CKD diet and tissue collection

CKD was induced by feeding a casein-based diet containing 0.6% calcium, 0.9% phosphate, and 0.2% adenine (Envigo, Teklad Co. Ltd) [(34)]. The CTL group received the same diet without adenine. At 13 weeks of age, all animals were sacrificed, and blood was obtained by cardiac puncture under terminal anesthesia. Femora, tibia, and kidneys were harvested and processed, and stored accordingly.

Serum and urine biochemistry

Blood was allowed to clot and then centrifuged at 2,500 xg for 10 min at 4°C and serum collected. Serum blood urea nitrogen (BUN), creatinine (Cr), calcium (Ca), phosphorus (Pi), and alkaline phosphatase (ALP) activity were quantified using a biochemistry analyzer (Beckman Coulter AU480, Olympus). Enzyme-linked immunosorbent assay (ELISA) kits were used to measure intact PTH (Pathway Diagnostics, Dorking, UK), FGF23 (Kainos Laboratories, Inc. Japan), N-terminal propeptide of human procollagen type I (PINP, Wuhan Fine Biotech, Wuhan, China), and carboxy-terminal telopeptide of type I collagen (αCTX, Wuhan Fine Biotech, Wuhan, China) levels according to the manufacturers' instructions. Before sacrifice, mice were housed in cages with hydrophobic bedding, LabSand (Coastline Global, CA, USA) for collecting urine samples. The Cr and albumin of urine samples were determined by semi-quantitative test strips (Microalbustix, Siemens) and the specific gravity (SG) of urine samples was determined by a handheld manual refractometer.

Histopathological analysis of kidney and bone tissues

The right tibiae and kidneys were fixed in 4% paraformaldehyde (PFA, for 24 hrs) and stored

in 70% ethanol. Kidney tissue was processed to paraffin wax using a Leica ASP300S tissue processor (Leica Microsystems, Milton Keynes, UK). Hematoxylin and eosin (H&E), Masson's trichrome, and von Kossa staining were performed according to standard methods. Histopathological scoring of renal interstitial inflammation, tubular atrophy, protein casts, and renal fibrosis was defined as 0 = normal; 1 = mild, involvement of < 25% of the cortex; 2 = moderate, involvement of 25 to 50% of the cortex; 3 = severe, involvement of 50 to 75% of the cortex; 4 = extensive, involvement of > 75% of the cortex. Bones were decalcified in 10% ethylenediaminetetraacetic acid (EDTA; pH 7.4) for 14 days at 4°C and then processed to paraffin wax. Sections, 3 μm in thickness were stained by Goldner's Trichrome and reacted for tartrate-resistant acid phosphatase (TRAP) using standard protocols [35]. All slides were imaged using a NanoZoomer XR slide scanning system (Hamamatsu Photonics, Japan). Bone histomorphometry was quantified using the BioQuant Osteo software (BIOQUANT Image Analysis Corporation, Texas, U.S.A.) using the approved ASBMR histomorphometry nomenclature (three sections/bone; six randomly selected bones from each group) [36].

Micro-computed tomography

The left tibia was dissected and stored at -20°C in distilled water pending analysis. The cortical geometry and trabecular microarchitecture were determined using a micro-computed tomography (μCT, Skyscan 1172 X-ray microtomography, Bruker, Kontich, Belgium) as described previously [37,38]. In brief, high-resolution scans with an isotropic voxel size of 5 μm were acquired (60 kV, 167 μA, and 0.5 mm filter, 0.6° rotation angle). The slices were then reconstructed using the NRecon 1.7.3.0 program (Bruker, Kontich, Belgium). CTAn software 1.15.4.0 (Skyscan) was used to visualize and determine bone histomorphometric parameters from the reconstructed image sets. Three-dimensional (3D) images were created using IMARIS 9.0.

Each tibia was aligned along its longitudinal axis and volume of interest (VOI) was analyzed using anatomical landmarks based on previous studies [39,40]. The selected trabecular (Tb) VOIs in the proximal tibial metaphysis began from the bottom of the growth plate, excluding the cortical shell, and extended distally 5% of the entire tibial length. A total of 250 slices beneath this 5% were selected to exclude the primary spongiosa. The cortical analysis was performed on datasets derived from μCT scan images at 37% and 50% of the total tibial length from the top of the tibia. Following segmentation, alignment, and removal of fibula from the dataset, a minimum bone threshold was selected for each bone to separate higher

density bone from soft tissues and air. BMD phantoms of known calcium hydroxyapatite mineral densities of 0.25 and 0.75 g/cm^3 were scanned and reconstructed using the same parameters as used for bone samples.

Primary calvarial osteoblast isolation and culture

Under sterile conditions, primary calvarial osteoblasts were obtained from 3 to 5-day-old C57BL/6 mice by sequential enzyme digestion [1 mg/ml collagenase type II (Worthington Biochemical, Lakewood, NJ, USA) in Hanks' balanced salt solution (Life Technologies, Paisley, UK); 4 mM EDTA] and expanded following standard procedures [41,42]. For individual studies, the cells were grown in a growth medium consisting of α-minimum essential medium (αMEM, Invitrogen, Paisley, UK) supplemented with 10% fetal bovine serum (FBS) (Life Technologies, Paisley, UK) and 0.5% gentamycin (Life Technologies) until confluent.

Establishment of Pi-substrate free mineralization model for primary osteoblast culture

To study the effects of varying Pi concentrations on phosphatase expression it was essential to control Pi concentration in the basal mineralizing medium. This ruled out the use of β-glycerophosphate (βGP) as the availability of Pi from βGP requires the action of TNAP [33] which can itself be modulated by CKD-associated endocrine factors such as Pi, PTH, and FGF23 [19,43,44]. Therefore, upon confluence (day 0), mineralization was induced by supplementing the growth medium (Ca, and Pi concentration in media: 1.8 mM and 1 mM, respectively) with 50 μg/ml L-ascorbic acid (AA) (Sigma-Aldrich, Dorset, UK) and 1.5 mM $CaCl_2$ (Sigma-Aldrich) [19]. Cultures were also supplemented with a range of Pi (Sigma-Aldrich; 1-5 mM), PTH (Sigma-Aldrich; 0-50 nM), and FGF23 (R&D Systems, Abington, UK; 0-200 ng/ml) with or without klotho (R&D Systems; 50ng/ml). Cells were maintained in a 5% CO_2 atmosphere at 37°C and mineralization media was changed every second/third day for 28 days.

Cell viability and cytotoxicity assay

To assess the effects of Pi on primary osteoblast cell viability, The AlamarBlue (resazurin reduction) assay (Thermo Fisher Scientific, Loughborough, UK), and lactate dehydrogenase (LDH) CytoTox 96 cytotoxicity assay (Promega, Southampton, UK) were performed as previously described [45,46]. Briefly, cells were seeded in 96 and 24 well plates respectively and after reaching confluency, the growth medium was exchanged for mineralization media

containing Pi (final concentration 1 - 5 mM) and treated for up to 28 days. The AlamarBlue fluorescence was read at excitation 530nm, emission 590nm on a BioTek Synergy microplate reader. The absorbance intensity at 490 nm was used to determine the LDH concentration released into the culture media.

RNA extraction and quantitative polymerase chain reaction

The distal and proximal epiphyses of the left femurs were excised, and the diaphyseal bone marrow was removed by centrifugation at 13,000 xg for 10 mins at 4°C. The resultant hollow cortical bone shafts were homogenized using a Rotor-Stator Homogenizer (Ultra-Turrax T10). RNA extraction from the homogenized bone and cultured primary osteoblasts was completed using the RNeasy kit (Qiagen). The RNA concentration was determined using a NanoDrop spectrophotometer (Fisher Scientific, Loughborough, UK) at a wavelength of 260 nm, and RNA purity was evaluated by the 260/280 nm ratio. RNA was reverse transcribed to complementary DNA (cDNA) using Superscript II (Invitrogen). All genes were analyzed with the SYBR green detection method (PCR Biosystems, UK) using the Stratagene Mx3000P real time QPCR system (Agilent Technologies, Santa Clara, CA, USA). Gene expression data were normalized against housekeeping genes (*Gapdh* in primary osteoblasts and *Atp5b* in bone tissue) using MxPro software (Cheshire, UK). The relative expression of the analyzed genes was calculated using the ΔΔCt method [47] and expressed as a fold change compared to CTL values. The sequences of the primers used in this study are listed in Supplementary Table S1.

Protein extraction and isolation from brush border membrane vesicles (BBMV) of kidney Kidneys were homogenized in ice-cold buffer A [50 mM D-mannitol (Sigma-Aldrich); 2 mM 4-(2-hydroxyethyl)-1-piperazineethanesulfonic acid (HEPES, Sigma-Aldrich); 2.5 mM ethylene glycol-bis (2-aminoethylether)-N, N, N', N'-tetraacetic acid (EGTA, Sigma-Aldrich), and 12 mM Tris-base (Fisher Bioreagents) titrated to pH 7.1] mixed with a protease inhibitor cocktail (Sigma-Aldrich, St. Louis, MO, USA). BBMVs were isolated from microvilli of kidneys using 2 consecutive magnesium precipitations in buffer A and then buffer B [150 mM D-mannitol, 2.5 mM EGTA, and 6 mM Tris hydrochloride (Tris-HCL, Sigma-Aldrich) as described previously [48,49]. The resultant BBMV pellet was resuspended in radioimmunoprecipitation assay (RIPA) buffer (Thermo Fisher Scientific, Paisley, UK) containing a protease inhibitor cocktail (Roche, Burgess Hill, UK).

Western blot analysis

Protein from cultured osteoblasts and right femoral diaphyseal bone (with marrow removed) was extracted in RIPA buffer containing protease inhibitor cocktail (Roche) after homogenization. Protein concentrations were determined using the BCA protein assay kit (Life Technologies). Equal amounts of extracted proteins were separated using a 10% Bis-Tris protein gel (Thermo Fisher Scientific). After blocking in 5% skimmed milk/Tris-buffered saline with Tween 20 (TBST) or LI-COR buffer at room temperature (RT) for 1 hour, the membranes were incubated sequentially with primary and secondary antibodies as described in Supplementary Tables S2 and S3. Western blot analysis of proteins from primary osteoblasts was performed using the Odyssey infrared detection system (LI-COR). Western blot analysis of proteins from bone tissues was undertaken using the ultra-sensitive enhanced chemiluminescence (ECL) detection system (Thermo Fisher Scientific). The blots were imaged by the GeneGnome XRQ chemiluminescence imaging system (Syngene, UK). Densitometry of the protein bands was analyzed with Image J software (NIH) for quantification.

Quantification of ECM mineralization

To examine the effects of Pi, PTH, and FGF23 exposure on ECM mineralization, cultured monolayers were fixed in 4 % PFA for 10 mins at RT and stained with aqueous 2 % (w/v) Alizarin red solution (Sigma-Aldrich) for 10 mins at RT. The bound stain was solubilized in 10 % cetylpyridinium chloride (Sigma-Aldrich) and the optical density of the eluted solution was measured by spectrophotometry at 570 nm.

Statistical analysis

Quantitative data are expressed as the mean ± standard error of the mean (S.E.M) of at least three biological replicates per experiment. The precise number (n) is indicated in the relevant table and figure legends. Statistical analysis was performed using a two-tailed Student's t-test or one-way analysis of variance (ANOVA) followed by Tukey's range test, as appropriate. Statistical analysis was implemented by the GraphPad Prism software. A $p < 0.05$ was considered to be significant and noted as "*". p values of < 0.01, < 0.001, and < 0.0001 were noted as "**", "***" and "****" respectively.

Results

Mice fed an adenine supplemented diet exhibit CKD-like characteristics

Mice fed the adenine supplemented (CKD) diet began losing bodyweight by week 1 ($p < 0.0001$) and after 5-weeks their bodyweight loss approached ~30% (Fig. 1B and Table 1). Four mice on the CKD diet lost > 30% bodyweight between 4 and 5 weeks and were removed from the study. Serum and urine analyte levels at the end of the study are shown in Table 1. The CKD mice presented with distinct polyuria accompanied by a decreased urine creatinine/serum creatinine ratio (UCr/SCr, $p < 0.0001$) and SG ($p < 0.0001$). Although serum ALP levels were comparable in CTL and CKD mice, serum levels of BUN, Cr, Ca, and Pi ($p < 0.0001$) were higher in CKD mice (Table 1). CKD mice also exhibited a 1.84-fold and 150-fold increase in PTH ($p < 0.01$), and FGF23 ($p < 0.0001$), respectively compared to the CTL group. A significant increase in PINP and αCTX was also noted in CKD mice compared to CTL mice, suggesting an increased bone remodeling rate in this CKD-MBD model (Table 1).

CKD mice display severe kidney damage and altered gene expression

Grossly, the kidney contour of CKD mice appeared distinctly irregular, which was indicative of atrophy in CKD (Figs. S1A, i & ii). Compared to the CTL group, the CKD mice exhibited a higher prevalence of atrophic and dilated tubules containing a moderate amount of proteinaceous material and dilated Bowman's space together with a significant invasion of inflammatory cells (Figs. S1A, iii - vi). Moreover, with Masson's trichrome (MT) and von Kossa (VK) staining, CKD kidneys exhibited typical features of adenine-induced tubulointerstitial nephropathy, including moderate to severe interstitial fibrosis (Figs. S1A, v & vi), and calcification of tubular structures (Figs. S1A, vii & viii), sometimes surrounded by neutrophils. The scoring of these histopathological findings was higher in CKD mice ($p < 0.001$) (Fig. S1B). Transcripts encoding kidney injury biomarkers *Lcn2* (protein; Ngal), and *Spp1* (protein; osteopontin (OPN)) [50,51], as well as *Fgf23*, were increased in CKD mice whereas *Slc34a1* (protein; NaPi-2a) expression was decreased (Fig. S2A). Protein expression of OPN and NaPi-2a by BBMV confirmed the transcript data (Fig. S2B). Collectively, these data demonstrate that mice fed an adenine-rich diet for 5 weeks developed CKD.

BMD and structural analysis of the CKD-MBD bone phenotype

Trabecular BMD, bone volume/tissue volume (BV/TV), connectivity density (Conn Dn.), and structural model index (SMI) of the tibiae were all decreased in CKD mice when compared to controls ($p < 0.05$, Figs. 2A, C). Cortical bone analysis at 37% and 50% of total tibial length, revealed that CKD mice exhibited increased BMD and porosity but decreased BV/TV,

thickness (Th), and cross-sectional area (CSA) ($p < 0.05$, Figs. 2B, C). The histomorphometric analysis confirmed the reduced trabecular BV/TV in the CKD mice ($p < 0.01$; Fig. 3A, i & ii, and Fig. 3B). The osteoid volume/bone volume (OV/BV) was increased in CKD mice confirming the impaired mineralization in this compartment ($p < 0.01$; Fig. 3A, iii & iv, and Fig 3B). Osteoclast number associated with trabecular bone within the primary spongiosa of CKD mice was increased ($p < 0.05$; Fig. 3A, v & vi and Fig. 3B); an observation consistent with decreased *Tnfrsf11b* (osteoprotegerin) expression ($p < 0.001$) in CKD bones (Fig. 4A).

PHOSPHO1 and TNAP expression are altered in bones of CKD mice

Phospho1 expression ($p < 0.01$) was increased and *Alpl* expression ($p < 0.001$) was decreased in the femur of CKD mice when compared to CTL mice. The expression of *Enpp1*, *Slc20a2*, *Ank*, *Bglap*, *Pdpn*, *Runx2*, *Bmp2*, *Npnt*, *and Tnfrsf11b* was decreased whereas femoral expression of *Fgf23,* and *Adipoq, were* increased in CKD mice when compared to CTL mice. The expression levels of *Spp1*, *Slc20a1*, *Anxa6*, *Sost*, *Acp5*, *and Tnfsf11* were unchanged in the femur of CKD mice (Fig. 4A). The increased *Phospho1* expression in femurs of CKD mice was confirmed at the protein level whereas no significant decrease in TNAP protein expression in femurs of CKD mice was detected (Figs. 4B, C). The increased cortical BMD in CKD mice (Fig. 2B) is consistent with the higher PHOSPHO1 expression in the cortical bone shafts despite being an unexpected phenotype in CKD (Figs. 4A, B). To determine if the higher PHOSPHO1 expression was driving the increased cortical bone mineralization we completed a further analysis of the cortical femur of PHOSPHO1 deficient (P1KO) mice maintained on the 0.2% adenine supplemented diet for 5-weeks. As previously noted, (Fig. 2B), the cortical BMD of WT CKD mice was increased ($p < 0.01$) compared to WT control (WT CTL) mice but this increase was not noted in P1KO CKD mice which had a BMD similar to their respective controls (P1KO CTL) but lower than the BMD of WT CTL mice (Fig. 5). The response of other structural parameters to CKD was also influenced by the absence of PHOSPHO1. The increased porosity and decreased BV/TV, CSA, and Th noted in WT CKD mice were all blunted in the P1KO CKD mice when compared to P1KO CTL mice (Fig. 5).

Pi, PTH, and FGF23 perturb the expression of key mineralization markers in primary osteoblasts

To determine the causes of the mineralization defects noted in the CKD mice, we investigated the direct effects of FGF23, PTH, and Pi on the expression of PHOSPHO1 and TNAP and other key regulators of mineralization by primary osteoblasts in cultures. Over 28 days, the basal Pi-substrate free mineralization media promoted matrix mineralization and PHOSPHO1 and TNAP expression in a temporal manner at both the gene and protein level confirming the suitability of this culture model for our purposes (Fig. S3).

At concentrations of 2 mM and above, Pi significantly down-regulated *Phospho1, Alpl, and Bglap* mRNA expression ($p < 0.01$, Fig. 6A). In contrast, *Enpp1*, *Spp1* and *Slc20a1* expression was increased at the higher Pi concentrations ($p < 0.05$, Fig. 6A). Cell viability as assessed by Alamar blue and LDH release was unaffected at all Pi concentrations tested (Fig. S4). PTH down-regulated *Phospho1*, *Alpl*, and *Bglap* expression when treated with PTH at 5 nM and above ($p < 0.01$, Fig. 6B). *Enpp1*, *Slc20a2*, and *Runx2* expression were also decreased but only at higher PTH concentrations ($p < 0.05$, Fig. 6B). FGF23 had little effect on the expression of the genes studied although both *Phospho1* and *Alpl* expression were decreased but only at the highest FGF23 concentrations ($p < 0.05$, Fig. 6C). The addition of Klotho to the FGF23 supplemented cultures had no further effects on gene expression when compared with FGF23 alone (Fig. S5)

The inhibition of PHOSPHO1 and TNAP protein expression by Pi and PTH reflected their respective changes in gene expression (Figs. 7A, B). However, after a 28-day exposure to FGF23, PHOSPHO1 and TNAP protein expression decreased in a concentration-dependent manner, this change did not reach statistical significance from control-treated cultures (Fig. 7C). A similar trend was observed in the presence of FGF23 and Klotho (Fig. S6A, B).

Pi, PTH, and FGF23 have differing effects on ECM mineralization in primary osteoblasts

On day 28 of culture, the addition of Pi, 3 mM and above, increased the formation of mineralized bone nodules in a dose-dependent manner ($p < 0.001$; Fig. 8A). In contrast, the addition of PTH inhibited ECM mineralization and this was noted at concentrations as low as 0.5 nM. Mineralization was completely abolished at 25 and 50 nM ($p < 0.001$, Fig. 8B). FGF23 with or without klotho had no effects on ECM mineralization of primary osteoblasts at the concentrations tested (Fig. 8C; Figs. S6C, D).

Discussion

The primary findings of this study are that (1) CKD mice develop modest - severe skeletal complications that are characteristic of renal osteodystrophy (ROD), a feature of CKD-MBD, and include decreased trabecular and cortical bone mass and elevated serum levels of Pi, PTH, and FGF23, (2) BMD of trabecular bone is decreased whereas it is increased in cortical bone of CKD mice, (3) the ROD phenotype is characterized by increased PHOSPHO1 expression in the cortical bone, and in the absence of PHOSPHO1 cortical BMD is unchanged in P1KO CKD mice, (4) Pi, PTH, and FGF23 have varying effects on osteoblast ECM mineralization but all three decrease PHOSPHO1 and TNAP expression in culture. Overall, utilizing *in vivo* and *in vitro* experimental models of CKD, this study is the first to implicate PHOSPHO1 and TNAP function in the altered mineralization status of bones in an animal model of CKD-MBD.

These data were obtained using the adenine-induced model of CKD which has been used previously in rodents to induce gradual and progressive kidney disease that is associated with a reduced renal clearance of circulating substances including BUN and Cr whose serum concentrations were 2 to 3-fold higher than controls [34,52]. In addition, adenine ingestion caused marked inflammatory cell infiltration into the tubulointerstitium, protein cast formation, and crystal deposition in the tubular lumen as previously reported [34]. The gene expression of *Spp1* and *Lcn* [51,53,54], which are indicative of rapid advancement to end-stage renal failure was dramatically upregulated in the adenine-fed mice. Loss of kidney function was also evidenced by the suppression of NaPi-2a expression by stimulation of the FGF23-αklotho signaling pathway [55]. Collectively, mice fed an adenine supplemented diet developed CKD with SHPT as well as high levels of circulating FGF23, and hyperphosphatemia, which corresponds in severity to approximately stage 3 of human CKD [56].

In humans, deteriorating renal function contributes to the progression of ROD which results in bone loss, osteoporosis, and eventually increased morbidity and mortality resulting from fractures and/or cardiovascular disease [57,58]. A similar bone phenotype was mirrored in this present study where cortical thinning, lower BV/TV, and increased cortical porosity were noted in the adenine-fed mice. The loss of bone is likely to be multi-factorial but PTH enhanced bone resorption via altered RANKL and OPG expression is likely to predominate [13,59]. In the early stages of CKD, the low bone turnover disease results from bone cell

inactivity due to PTH resistance, as well as reduced calcitriol levels, and accumulation of uremic toxins [60-62]. When renal function further deteriorates, the chronically increased PTH levels overcome peripheral PTH resistance and activate the indolent bone cells, leading to high turnover bone disease (osteitis fibrosa) [8]. Bone resorption predominates in both high and low bone turnover disease and the resultant elevated serum Ca and Pi levels promote bone extra-skeletal (vascular) calcification [7]. In agreement with the results of this present study, others have also reported increased porosity and compromised bone architecture in CKD animal models although inconsistent effects on the cortical and trabecular compartments have been reported [34,63-67]. Similarly, inconsistencies in trabecular and cortical BMD in CKD animal models also exist [68,69]. Specifically, in a mouse nephrectomy model in which serum Pi levels were unchanged, trabecular and cortical BMD were increased and decreased, respectively which was the opposite to that found in this present study [69]. The spectrum of bone phenotypes reported in CKD-MBD models may reflect the differing serum PTH levels at the point of study as progressive SHPT is associated with different effects on bone quality and structure [66].

The high bone turnover status in SHPT will contribute to bone that is less mineralized, a hallmark of stage 4 and 5 CKD, and lead to reduced mechanical strength and increased risk of fractures [8,70]. Similarly, in this present study, PTH induced skeletal remodeling is likely to, at least in part, explain the poorly mineralized trabecular bone noted in this study although PTH exposure can also inhibit osteoblast differentiation and thus indirectly delay osteoid production and matrix mineralization [71,72]. Additionally, the CKD-driven increase in osteocyte secretion of Wnt/β-catenin signaling inhibitors, such as FGF23, Dickkopf 1, and sclerostin may negatively affect osteoblast function and contribute to the mineralization defect in ROD [4,17,44,68,73-76]. The results of this present study offer changes to PHOSPHO1 and TNAP osteoblast expression as an additional/alternative explanation for the altered bone mineralization status associated with ROD.

Monitoring serum ALP has been regarded as a useful serum marker of bone turnover in ROD however its expression in bone, functioning as a phosphatase capable of mineralizing osteoid has not to our knowledge been explored in the pathogenesis of ROD [77]. The decreased *Alpl* expression in CKD cortical bone was not however consistent with the observed increased cortical BMD and we hypothesized that the latter was possibly driven by increased PHOSPHO1 expression [33]. To examine this further we determined cortical BMD and other

structural parameters in P1KO CKD mice. In the absence of PHOSPHO1, cortical BMD was unchanged, and surprisingly other structural parameters were improved in P1KO CKD mice. Whilst supportive of our hypothesis, the mechanisms responsible for the increased PHOSPHO1 in cortical bone are unclear and cannot be explained by the direct effects of Pi, FGF23, and PTH which are all inhibitory to PHOSPHO1 expression as shown in this and other studies [18-20]. A compensatory mechanism in an attempt to protect the bone from hypomineralization may be a possibility but further work on this and whether PHOSPHO1 deficiency improves bone health in ROD by decreasing cortical porosity is warranted [78,79]. The decreased cortical bone TNAP expression could be a direct effect of Pi and PTH on osteoblasts as shown by the *in vitro* data of this and other studies [80,81]. Furthermore, whilst not observed in this study, others have reported a direct inhibitory effect of FGF23 on osteoblast matrix mineralization which may be mediated by decreased TNAP expression and an accumulation of PPi, a potent inhibitor of mineralization [17,44,82,83]. However, indirect systemic effects via disrupted vitamin D status and Pi and Ca metabolism are also likely to contribute to the altered TNAP expression in bone of CKD-MBD mice [84,85].

Several studies have reported that mineralizing cells including odontoblasts, chondrocytes, and osteoblasts are sensitive to P_i and respond by altering the expression of mineralization-associated genes and transcription factors [86-89]. The regulation of biomineralization by Pi may be related to its ability to stimulate MV release and/or the accumulation of type III NaP(i) transporter (PiT1) in osteoblasts promoting Pi uptake and ECM mineralization [90,91]. In relation to this present study, the availability of exogenous Pi to promote osteoblast matrix mineralization by-passes the requirement for Pi production from PCho and PEA by PHOSPHO1 and PPi by TNAP [92-94] and may explain the concentration-dependent decrease in PHOSPHO1 and TNAP expression by exogenous Pi as part of a negative feedback mechanism [86,95]. In this regard, human PHOSPHO1 shares approximately 30% homology at the amino acid level with a tomato phosphate starvation-induced gene (LePS2) whereby phosphatase activity converts organic phosphorus into available Pi. LePS2 expression is tightly regulated by Pi availability where it is induced in the absence of Pi, but repressed in the presence of Pi [96,97]. It is unknown if such a Pi negative feedback mechanism operates *in vivo* to control PHOSPHO1 expression but if so, it could not explain the increased PHOSPHO1 expression in the high Pi conditions noted in the CKD mice. Notwithstanding this, it is recognized that high Pi levels can modulate osteoclast activity and osteoblast proliferation, differentiation, and apoptosis which may contribute to the altered skeletal

architecture of the CKD mice found in this study [89,98].

In summary, this study has shown that PHOSPHO1 and TNAP, two phosphatases required for bone mineralization, have altered expression in the bones of CKD-MBD mice which may help explain the aberrant mineralization status of trabecular and cortical bone. The altered PHOSPHO1 and TNAP expression may be a direct result of the altered endocrine milieu, or due to disrupted Pi and Ca metabolism. These novel findings provide a foundation for future research to explore potential therapies to improve bone health in CKD-MBD.

Acknowledgments

This work was funded by the Tri-Service General Hospital (TSGH), National Defense Medical Center (NDMC), Taiwan through a Ph.D. scholarship award to SNH. We are also grateful to the Biotechnology and Biological Sciences Research Council (BBSRC) for Institute Strategic Programme Grant Funding BB/J004316/1 to CF, LAS & VEM and grant DE12889 from the National Institute of Dental and Craniofacial Research (NIDCR) to JLM. We thank Elaine Seawright for technical assistance; Darren Smith, Tricia Mathieson, Heather Warnock, Lorraine Blackford, Lee Mcmanus, and the staff of the animal care facility at Biological Research Facility (BRF) providing animal support; Colin Wood and the staff at Easter Bush Pathology, Royal (Dick) School of Veterinary Studies, University of Edinburgh for conducting mouse serum biochemistries.

Disclosures

All authors state that they have no conflicts of interest.

Data availability statement

All data supporting the findings of this study are available either within the article or the supplementary information.

Authors' contributions

Conception and design of the study: SNH, CF, VEM, AN & KAS. Acquisition of data: SNH, LAS, SD, EM. Interpretation of data: SNH, LAS, SD, JLM, EM, and KAS, CF. Drafting the manuscript: SNH, CF. Revising the manuscript and final approval, and agreement to be accountable for all aspects of the work: all authors.

References

1. Patel SS, Kimmel PL, Singh A. New clinical practice guidelines for chronic kidney disease: a framework for K/DOQI. Seminars in nephrology. Nov 2002;22(6):449-58. Epub 2002/11/14.
2. Gutiérrez OM. Fibroblast growth factor 23 and disordered vitamin D metabolism in chronic kidney disease: updating the "trade-off" hypothesis. Clinical journal of the American Society of Nephrology : CJASN. Sep 2010;5(9):1710-6. Epub 2010/05/29.
3. Moe S, Drüeke T, Cunningham J, Goodman W, Martin K, Olgaard K, et al. Definition, evaluation, and classification of renal osteodystrophy: a position statement from Kidney Disease: Improving Global Outcomes (KDIGO). Kidney international. Jun 2006;69(11):1945-53. Epub 2006/04/28.
4. Fang Y, Ginsberg C, Sugatani T, Monier-Faugere MC, Malluche H, Hruska KA. Early chronic kidney disease-mineral bone disorder stimulates vascular calcification. Kidney international. Jan 2014;85(1):142-50. Epub 2013/07/26.
5. Kazama JJ, Iwasaki Y, Fukagawa M. Uremic osteoporosis. Kidney international supplements. Dec 2013;3(5):446-50. Epub 2014/07/16.
6. Wesseling-Perry K. Bone disease in pediatric chronic kidney disease. Pediatric nephrology (Berlin, Germany). Apr 2013;28(4):569-76. Epub 2012/10/16.
7. Zheng CM, Zheng JQ, Wu CC, Lu CL, Shyu JF, Yung-Ho H, et al. Bone loss in chronic kidney disease: Quantity or quality? Bone. Jun 2016;87:57-70. Epub 2016/04/07.
8. Drüeke TB, Massy ZA. Changing bone patterns with progression of chronic kidney disease. Kidney international. Feb 2016;89(2):289-302. Epub 2016/01/26.
9. Mirza MA, Hansen T, Johansson L, Ahlström H, Larsson A, Lind L, et al. Relationship between circulating FGF23 and total body atherosclerosis in the community. Nephrology, dialysis, transplantation : official publication of the European Dialysis and Transplant Association - European Renal Association. Oct 2009;24(10):3125-31. Epub 2009/05/12.
10. Shimada T, Kakitani M, Yamazaki Y, Hasegawa H, Takeuchi Y, Fujita T, et al. Targeted ablation of Fgf23 demonstrates an essential physiological role of FGF23 in phosphate and vitamin D metabolism. The Journal of clinical investigation. 2004;113(4):561-8.
11. Stubbs J, Liu S, Quarles LD. PHOSPHORUS METABOLISM AND MANAGEMENT IN CHRONIC KIDNEY DISEASE: Role of Fibroblast Growth Factor 23 in Phosphate Homeostasis and Pathogenesis of Disordered Mineral Metabolism in Chronic Kidney Disease. Seminars in dialysis. https://doi.org/10.1111/j.1525-139X.2007.00308.x 2007/07/01 2007;20(4):302-8.
12. Eriksen EF. Primary hyperparathyroidism: lessons from bone histomorphometry. Journal of bone and mineral research : the official journal of the American Society for Bone and Mineral Research. Nov 2002;17 Suppl 2:N95-7. Epub 2002/11/05.
13. Ma YL, Cain RL, Halladay DL, Yang X, Zeng Q, Miles RR, et al. Catabolic effects of continuous human PTH (1--38) in vivo is associated with sustained stimulation of RANKL and inhibition of osteoprotegerin and gene-associated bone formation. Endocrinology. Sep 2001;142(9):4047-54. Epub 2001/08/23.
14. Graciolli FG, Neves KR, Barreto F, Barreto DV, Dos Reis LM, Canziani ME, et al. The complexity of chronic kidney disease-mineral and bone disorder across stages of chronic kidney disease. Kidney international. Jun 2017;91(6):1436-46. Epub 2017/03/21.

15. Quarles LD. A systems biology preview of the relationships between mineral and metabolic complications in chronic kidney disease. Seminars in nephrology. Mar 2013;33(2):130-42. Epub 2013/03/08.
16. Peacock M. Phosphate Metabolism in Health and Disease. Calcified tissue international. Jan 2021;108(1):3-15. Epub 2020/04/09.
17. Murali SK, Andrukhova O, Clinkenbeard EL, White KE, Erben RG. Excessive Osteocytic Fgf23 Secretion Contributes to Pyrophosphate Accumulation and Mineralization Defect in Hyp Mice. PLoS biology. Apr 2016;14(4):e1002427. Epub 2016/04/02.
18. Allan EH, Häusler KD, Wei T, Gooi JH, Quinn JM, Crimeen-Irwin B, et al. EphrinB2 regulation by PTH and PTHrP revealed by molecular profiling in differentiating osteoblasts. Journal of bone and mineral research : the official journal of the American Society for Bone and Mineral Research. Aug 2008;23(8):1170-81. Epub 2008/07/17.
19. Houston DA, Myers K, MacRae VE, Staines KA, Farquharson C. The Expression of PHOSPHO1, nSMase2 and TNAP is Coordinately Regulated by Continuous PTH Exposure in Mineralising Osteoblast Cultures. Calcified tissue international. Nov 2016;99(5):510-24. Epub 2016/07/23.
20. St John HC, Meyer MB, Benkusky NA, Carlson AH, Prideaux M, Bonewald LF, et al. The parathyroid hormone-regulated transcriptome in osteocytes: parallel actions with 1,25-dihydroxyvitamin D3 to oppose gene expression changes during differentiation and to promote mature cell function. Bone. Mar 2015;72:81-91. Epub 2014/12/03.
21. Millán JL. The role of phosphatases in the initiation of skeletal mineralization. Calcified tissue international. Oct 2013;93(4):299-306. Epub 2012/11/28.
22. Dillon S, Staines KA, Millán JL, Farquharson C. How To Build a Bone: PHOSPHO1, Biomineralization, and Beyond. JBMR plus. Jul 2019;3(7):e10202. Epub 2019/08/03.
23. Houston B, Stewart AJ, Farquharson C. PHOSPHO1-A novel phosphatase specifically expressed at sites of mineralisation in bone and cartilage. Bone. Apr 2004;34(4):629-37. Epub 2004/03/31.
24. Houston B, Seawright E, Jefferies D, Hoogland E, Lester D, Whitehead C, et al. Identification and cloning of a novel phosphatase expressed at high levels in differentiating growth plate chondrocytes. Biochimica et biophysica acta. Jan 11 1999;1448(3):500-6. Epub 1999/02/17.
25. Roberts S, Narisawa S, Harmey D, Millan JL, Farquharson C. Functional involvement of PHOSPHO1 in matrix vesicle-mediated skeletal mineralization. Journal of bone and mineral research : the official journal of the American Society for Bone and Mineral Research. Apr 2007;22(4):617-27. Epub 2007/01/18.
26. Huesa C, Yadav MC, Finnila MA, Goodyear SR, Robins SP, Tanner KE, et al. PHOSPHO1 is essential for mechanically competent mineralization and the avoidance of spontaneous fractures. Bone. May 01 2011;48(5):1066-74. Epub 2011/01/29.
27. Boyde A, Staines KA, Javaheri B, Millan JL, Pitsillides AA, Farquharson C. A distinctive patchy osteomalacia characterises Phospho1-deficient mice. J Anat. Aug 2017;231(2):298-308. Epub 2017/07/25.
28. Bernard GW. Ultrastructural localization of alkaline phosphatase in initial intramembranous osteogenesis. Clinical orthopaedics and related research. Sep 1978(135):218-25. Epub 1978/09/01.
29. Vimalraj S. Alkaline phosphatase: Structure, expression and its function in bone mineralization. Gene. Jun 6 2020;754:144855. Epub 2020/06/12.
30. Hessle L, Johnson KA, Anderson HC, Narisawa S, Sali A, Goding JW, et al. Tissue-nonspecific alkaline phosphatase and plasma cell membrane glycoprotein-1 are

central antagonistic regulators of bone mineralization. Proceedings of the National Academy of Sciences of the United States of America. Jul 9 2002;99(14):9445-9. Epub 2002/06/26.

31. Whyte MP. Chapter 73 - Hypophosphatasia: Nature's Window on Alkaline Phosphatase Function in Humans. In: Bilezikian JP, Raisz LG, Martin TJ, editors. Principles of Bone Biology (Third Edition). San Diego: Academic Press; 2008. p. 1573-98.
32. Yadav MC, Simao AM, Narisawa S, Huesa C, McKee MD, Farquharson C, et al. Loss of skeletal mineralization by the simultaneous ablation of PHOSPHO1 and alkaline phosphatase function: a unified model of the mechanisms of initiation of skeletal calcification. Journal of bone and mineral research : the official journal of the American Society for Bone and Mineral Research. Feb 2011;26(2):286-97. Epub 2010/08/05.
33. Huesa C, Houston D, Kiffer-Moreira T, Yadav MM, Millan JL, Farquharson C. The Functional co-operativity of Tissue-Nonspecific Alkaline Phosphatase (TNAP) and PHOSPHO1 during initiation of Skeletal Mineralization. Biochemistry and biophysics reports. Dec 01 2015;4:196-201. Epub 2015/10/13.
34. Jia T, Olauson H, Lindberg K, Amin R, Edvardsson K, Lindholm B, et al. A novel model of adenine-induced tubulointerstitial nephropathy in mice. BMC nephrology. May 30 2013;14:116. Epub 2013/05/31.
35. Staines KA, Hopkinson M, Dillon S, Stephen LA, Fleming R, Sophocleous A, et al. Conditional deletion of E11/Podoplanin in bone protects against ovariectomy-induced increases in osteoclast formation and activity. Bioscience reports. Jan 31 2020;40(1). Epub 2020/01/03.
36. Dempster DW, Compston JE, Drezner MK, Glorieux FH, Kanis JA, Malluche H, et al. Standardized nomenclature, symbols, and units for bone histomorphometry: a 2012 update of the report of the ASBMR Histomorphometry Nomenclature Committee. Journal of bone and mineral research : the official journal of the American Society for Bone and Mineral Research. Jan 2013;28(1):2-17. Epub 2012/12/01.
37. Javaheri B, Carriero A, Staines KA, Chang YM, Houston DA, Oldknow KJ, et al. Phospho1 deficiency transiently modifies bone architecture yet produces consistent modification in osteocyte differentiation and vascular porosity with ageing. Bone. Dec 2015;81:277-91. Epub 2015/08/02.
38. Staines KA, Javaheri B, Hohenstein P, Fleming R, Ikpegbu E, Unger E, et al. Hypomorphic conditional deletion of E11/Podoplanin reveals a role in osteocyte dendrite elongation. Journal of cellular physiology. Nov 2017;232(11):3006-19. Epub 2017/05/11.
39. Fritton JC, Myers ER, Wright TM, van der Meulen MC. Loading induces site-specific increases in mineral content assessed by microcomputed tomography of the mouse tibia. Bone. Jun 2005;36(6):1030-8. Epub 2005/05/10.
40. Main RP, Lynch ME, van der Meulen MC. Load-induced changes in bone stiffness and cancellous and cortical bone mass following tibial compression diminish with age in female mice. The Journal of experimental biology. May 15 2014;217(Pt 10):1775-83. Epub 2014/03/01.
41. Jonason JH, O'Keefe RJ. Isolation and culture of neonatal mouse calvarial osteoblasts. Methods in molecular biology (Clifton, NJ). 2014;1130:295-305. Epub 2014/02/01.
42. Orriss IR, Hajjawi MO, Huesa C, MacRae VE, Arnett TR. Optimisation of the differing conditions required for bone formation in vitro by primary osteoblasts from mice and rats. International journal of molecular medicine. Nov 2014;34(5):1201-8. Epub 2014/09/10.

43. Rendenbach C, Yorgan TA, Heckt T, Otto B, Baldauf C, Jeschke A, et al. Effects of extracellular phosphate on gene expression in murine osteoblasts. Calcified tissue international. May 2014;94(5):474-83. Epub 2013/12/25.
44. Shalhoub V, Ward SC, Sun B, Stevens J, Renshaw L, Hawkins N, et al. Fibroblast growth factor 23 (FGF23) and alpha-klotho stimulate osteoblastic MC3T3.E1 cell proliferation and inhibit mineralization. Calcified tissue international. Aug 2011;89(2):140-50. Epub 2011/06/03.
45. O'Brien J, Wilson I, Orton T, Pognan F. Investigation of the Alamar Blue (resazurin) fluorescent dye for the assessment of mammalian cell cytotoxicity. European journal of biochemistry. Sep 2000;267(17):5421-6. Epub 2000/08/22.
46. Decker T, Lohmann-Matthes ML. A quick and simple method for the quantitation of lactate dehydrogenase release in measurements of cellular cytotoxicity and tumor necrosis factor (TNF) activity. Journal of immunological methods. Nov 25 1988;115(1):61-9. Epub 1988/11/25.
47. Livak KJ, Schmittgen TD. Analysis of relative gene expression data using real-time quantitative PCR and the 2(-Delta Delta C(T)) Method. Methods (San Diego, Calif). Dec 2001;25(4):402-8. Epub 2002/02/16.
48. Biber J, Stieger B, Stange G, Murer H. Isolation of renal proximal tubular brush-border membranes. Nature protocols. 2007;2(6):1356-9. Epub 2007/06/05.
49. Booth AG, Kenny AJ. A rapid method for the preparation of microvilli from rabbit kidney. The Biochemical journal. Sep 1974;142(3):575-81. Epub 1974/09/01.
50. Viau A, El Karoui K, Laouari D, Burtin M, Nguyen C, Mori K, et al. Lipocalin 2 is essential for chronic kidney disease progression in mice and humans. The Journal of clinical investigation. Nov 2010;120(11):4065-76. Epub 2010/10/06.
51. Kaleta B. The role of osteopontin in kidney diseases. Inflammation research : official journal of the European Histamine Research Society [et al]. Feb 2019;68(2):93-102. Epub 2018/11/21.
52. Tamura M, Aizawa R, Hori M, Ozaki H. Progressive renal dysfunction and macrophage infiltration in interstitial fibrosis in an adenine-induced tubulointerstitial nephritis mouse model. Histochemistry and Cell Biology. 2009/04/01 2009;131(4):483-90.
53. Viau A, El Karoui K, Laouari D, Burtin M, Nguyen C, Mori K, et al. Lipocalin 2 is essential for chronic kidney disease progression in mice and humans. The Journal of clinical investigation. 11/01/ 2010;120(11):4065-76.
54. Sugiura H, Matsushita A, Futaya M, Teraoka A, Akiyama KI, Usui N, et al. Fibroblast growth factor 23 is upregulated in the kidney in a chronic kidney disease rat model. PloS one. 2018;13(3):e0191706. Epub 2018/03/09.
55. Hu MC, Shiizaki K, Kuro-o M, Moe OW. Fibroblast Growth Factor 23 and Klotho: Physiology and Pathophysiology of an Endocrine Network of Mineral Metabolism. Annual review of physiology. 2013/02/10 2013;75(1):503-33.
56. Levey AS, Coresh J, Balk E, Kausz AT, Levin A, Steffes MW, et al. National Kidney Foundation practice guidelines for chronic kidney disease: evaluation, classification, and stratification. Annals of internal medicine. Jul 15 2003;139(2):137-47. Epub 2003/07/16.
57. Jankowski J, Floege J, Fliser D, Böhm M, Marx N. Cardiovascular Disease in Chronic Kidney Disease. Circulation. 2021/03/16 2021;143(11):1157-72.
58. Gal-Moscovici A, Sprague SM. Bone health in chronic kidney disease-mineral and bone disease. Advances in chronic kidney disease. Jan 2007;14(1):27-36. Epub 2007/01/04.
59. Huang JC, Sakata T, Pfleger LL, Bencsik M, Halloran BP, Bikle DD, et al. PTH

differentially regulates expression of RANKL and OPG. Journal of bone and mineral research : the official journal of the American Society for Bone and Mineral Research. Feb 2004;19(2):235-44. Epub 2004/02/19.
60. Couttenye MM, D'Haese PC, Verschoren WJ, Behets GJ, Schrooten I, De Broe ME. Low bone turnover in patients with renal failure. Kidney international. 1999/12/01/ 1999;56:S70-S6.
61. Malluche HH, Mawad H, Monier-Faugere M-C. The importance of bone health in end-stage renal disease: out of the frying pan, into the fire? Nephrology Dialysis Transplantation. 2004;19(suppl_1):i9-i13.
62. Massy Z, Drueke T. Adynamic bone disease is a predominant bone pattern in early stages of chronic kidney disease. Journal of nephrology. Oct 2017;30(5):629-34. Epub 2017/04/14.
63. Tatsumoto N, Arioka M, Yamada S, Takahashi-Yanaga F, Tokumoto M, Tsuruya K, et al. Inhibition of GSK-3beta increases trabecular bone volume but not cortical bone volume in adenine-induced uremic mice with severe hyperparathyroidism. Physiological reports. Nov 2016;4(21). Epub 2016/11/03.
64. Zhang Q, Liu L, Lin W, Yin S, Duan A, Liu Z, et al. Rhein reverses Klotho repression via promoter demethylation and protects against kidney and bone injuries in mice with chronic kidney disease. Kidney international. Jan 2017;91(1):144-56. Epub 2016/10/04.
65. Lin W, Li Y, Chen F, Yin S, Liu Z, Cao W. Klotho preservation via histone deacetylase inhibition attenuates chronic kidney disease-associated bone injury in mice. Scientific reports. Apr 7 2017;7:46195. Epub 2017/04/08.
66. Miller MA, Chin J, Miller SC, Fox J. Disparate effects of mild, moderate, and severe secondary hyperparathyroidism on cancellous and cortical bone in rats with chronic renal insufficiency. Bone. 1998/09/01/ 1998;23(3):257-66.
67. Metzger CE, Swallow EA, Stacy AJ, Allen MR. Adenine-induced chronic kidney disease induces a similar skeletal phenotype in male and female C57BL/6 mice with more severe deficits in cortical bone properties of male mice. PloS one. 2021;16(4):e0250438.
68. Tani T, Orimo H, Shimizu A, Tsuruoka S. Development of a novel chronic kidney disease mouse model to evaluate the progression of hyperphosphatemia and associated mineral bone disease. Scientific reports. May 22 2017;7(1):2233. Epub 2017/05/24.
69. Lau WL, Linnes M, Chu EY, Foster BL, Bartley BA, Somerman MJ, et al. High phosphate feeding promotes mineral and bone abnormalities in mice with chronic kidney disease. Nephrology, dialysis, transplantation : official publication of the European Dialysis and Transplant Association - European Renal Association. Jan 2013;28(1):62-9. Epub 2012/10/10.
70. Goldenstein PT, Jamal SA, Moysés RM. Fractures in chronic kidney disease: pursuing the best screening and management. Current opinion in nephrology and hypertension. Jul 2015;24(4):317-23. Epub 2015/06/08.
71. Qin L, Raggatt LJ, Partridge NC. Parathyroid hormone: a double-edged sword for bone metabolism. Trends in endocrinology and metabolism: TEM. Mar 2004;15(2):60-5. Epub 2004/03/24.
72. Hock JM, Gera I. Effects of continuous and intermittent administration and inhibition of resorption on the anabolic response of bone to parathyroid hormone. Journal of bone and mineral research : the official journal of the American Society for Bone and Mineral Research. Jan 1992;7(1):65-72. Epub 1992/01/01.
73. Poole KE, van Bezooijen RL, Loveridge N, Hamersma H, Papapoulos SE, Löwik CW,

et al. Sclerostin is a delayed secreted product of osteocytes that inhibits bone formation. FASEB journal : official publication of the Federation of American Societies for Experimental Biology. Nov 2005;19(13):1842-4. Epub 2005/08/27.

74. Evenepoel P, D'Haese P, Brandenburg V. Sclerostin and DKK1: new players in renal bone and vascular disease. Kidney international. Aug 2015;88(2):235-40. Epub 2015/06/18.
75. Sabbagh Y, Graciolli FG, O'Brien S, Tang W, dos Reis LM, Ryan S, et al. Repression of osteocyte Wnt/β-catenin signaling is an early event in the progression of renal osteodystrophy. Journal of bone and mineral research : the official journal of the American Society for Bone and Mineral Research. Aug 2012;27(8):1757-72. Epub 2012/04/12.
76. Carrillo-Lopez N, Panizo S, Alonso-Montes C, Roman-Garcia P, Rodriguez I, Martinez-Salgado C, et al. Direct inhibition of osteoblastic Wnt pathway by fibroblast growth factor 23 contributes to bone loss in chronic kidney disease. Kidney international. Jul 2016;90(1):77-89. Epub 2016/05/12.
77. Bervoets AR, Spasovski GB, Behets GJ, Dams G, Polenakovic MH, Zafirovska K, et al. Useful biochemical markers for diagnosing renal osteodystrophy in predialysis end-stage renal failure patients. American journal of kidney diseases : the official journal of the National Kidney Foundation. May 2003;41(5):997-1007. Epub 2003/05/02.
78. Metzger CE, Swallow EA, Stacy AJ, Tippen SP, Hammond MA, Chen NX, et al. Reversing cortical porosity: Cortical pore infilling in preclinical models of chronic kidney disease. Bone. Feb 2021;143:115632. Epub 2020/09/15.
79. Metzger CE, Swallow EA, Allen MR. Elevations in Cortical Porosity Occur Prior to Significant Rise in Serum Parathyroid Hormone in Young Female Mice with Adenine-Induced CKD. Calcified tissue international. Apr 2020;106(4):392-400. Epub 2019/12/14.
80. Zerega B, Cermelli S, Bianco P, Cancedda R, Cancedda FD. Parathyroid hormone [PTH(1-34)] and parathyroid hormone-related protein [PTHrP(1-34)] promote reversion of hypertrophic chondrocytes to a prehypertrophic proliferating phenotype and prevent terminal differentiation of osteoblast-like cells. Journal of bone and mineral research : the official journal of the American Society for Bone and Mineral Research. Aug 1999;14(8):1281-9. Epub 1999/08/24.
81. van der Horst G, Farih-Sips H, Löwik CW, Karperien M. Multiple mechanisms are involved in inhibition of osteoblast differentiation by PTHrP and PTH in KS483 Cells. Journal of bone and mineral research : the official journal of the American Society for Bone and Mineral Research. Dec 2005;20(12):2233-44. Epub 2005/11/19.
82. Murali SK, Roschger P, Zeitz U, Klaushofer K, Andrukhova O, Erben RG. FGF23 Regulates Bone Mineralization in a 1,25(OH)2 D3 and Klotho-Independent Manner. Journal of bone and mineral research : the official journal of the American Society for Bone and Mineral Research. Jan 2016;31(1):129-42. Epub 2015/08/04.
83. Wang H, Yoshiko Y, Yamamoto R, Minamizaki T, Kozai K, Tanne K, et al. Overexpression of Fibroblast Growth Factor 23 Suppresses Osteoblast Differentiation and Matrix Mineralization In Vitro. Journal of Bone and Mineral Research. https://doi.org/10.1359/jbmr.080220 2008/06/01 2008;23(6):939-48.
84. Bover J, Ureña P, Aguilar A, Mazzaferro S, Benito S, López-Báez V, et al. Alkaline Phosphatases in the Complex Chronic Kidney Disease-Mineral and Bone Disorders. Calcified tissue international. Aug 2018;103(2):111-24. Epub 2018/02/16.
85. Andrukhova O, Schüler C, Bergow C, Petric A, Erben RG. Augmented Fibroblast Growth Factor-23 Secretion in Bone Locally Contributes to Impaired Bone

Mineralization in Chronic Kidney Disease in Mice. Frontiers in endocrinology. 2018;9:311. Epub 2018/06/27.
86. Foster BL, Nociti FH, Jr., Swanson EC, Matsa-Dunn D, Berry JE, Cupp CJ, et al. Regulation of cementoblast gene expression by inorganic phosphate in vitro. Calcified tissue international. Feb 2006;78(2):103-12. Epub 2006/02/10.
87. Julien M, Khoshniat S, Lacreusette A, Gatius M, Bozec A, Wagner EF, et al. Phosphate-dependent regulation of MGP in osteoblasts: role of ERK1/2 and Fra-1. Journal of bone and mineral research : the official journal of the American Society for Bone and Mineral Research. Nov 2009;24(11):1856-68. Epub 2009/05/08.
88. Julien M, Magne D, Masson M, Rolli-Derkinderen M, Chassande O, Cario-Toumaniantz C, et al. Phosphate stimulates matrix Gla protein expression in chondrocytes through the extracellular signal regulated kinase signaling pathway. Endocrinology. Feb 2007;148(2):530-7. Epub 2006/10/28.
89. Khoshniat S, Bourgine A, Julien M, Weiss P, Guicheux J, Beck L. The emergence of phosphate as a specific signaling molecule in bone and other cell types in mammals. Cellular and molecular life sciences : CMLS. Jan 2011;68(2):205-18. Epub 2010/09/18.
90. Chaudhary SC, Kuzynski M, Bottini M, Beniash E, Dokland T, Mobley CG, et al. Phosphate induces formation of matrix vesicles during odontoblast-initiated mineralization in vitro. Matrix biology : journal of the International Society for Matrix Biology. May-Jul 2016;52-54:284-300. Epub 2016/02/18.
91. Yoshiko Y, Candeliere GA, Maeda N, Aubin JE. Osteoblast autonomous Pi regulation via Pit1 plays a role in bone mineralization. Mol Cell Biol. Jun 2007;27(12):4465-74. Epub 2007/04/18.
92. Bellows CG, Heersche JN, Aubin JE. Inorganic phosphate added exogenously or released from beta-glycerophosphate initiates mineralization of osteoid nodules in vitro. Bone and mineral. Apr 1992;17(1):15-29. Epub 1992/04/01.
93. Roberts SJ, Stewart AJ, Sadler PJ, Farquharson C. Human PHOSPHO1 exhibits high specific phosphoethanolamine and phosphocholine phosphatase activities. The Biochemical journal. Aug 15 2004;382(Pt 1):59-65. Epub 2004/06/04.
94. Ciancaglini P, Yadav MC, Simão AM, Narisawa S, Pizauro JM, Farquharson C, et al. Kinetic analysis of substrate utilization by native and TNAP-, NPP1-, or PHOSPHO1-deficient matrix vesicles. Journal of bone and mineral research : the official journal of the American Society for Bone and Mineral Research. Apr 2010;25(4):716-23. Epub 2009/10/31.
95. Johnson KA, Hessle L, Vaingankar S, Wennberg C, Mauro S, Narisawa S, et al. Osteoblast tissue-nonspecific alkaline phosphatase antagonizes and regulates PC-1. American journal of physiology Regulatory, integrative and comparative physiology. Oct 2000;279(4):R1365-77. Epub 2000/09/27.
96. Baldwin JC, Karthikeyan AS, Raghothama KG. LEPS2, a phosphorus starvation-induced novel acid phosphatase from tomato. Plant physiology. Feb 2001;125(2):728-37. Epub 2001/02/13.
97. Stenzel I, Ziethe K, Schurath J, Hertel SC, Bosse D, Köck M. Differential expression of the LePS2 phosphatase gene family in response to phosphate availability, pathogen infection and during development. Physiologia plantarum. May 2003;118(1):138-46. Epub 2003/04/19.
98. Adams CS, Mansfield K, Perlot RL, Shapiro IM. Matrix regulation of skeletal cell apoptosis. Role of calcium and phosphate ions. The Journal of biological chemistry. Jun 8 2001;276(23):20316-22. Epub 2001/03/30.

Table 1. Body weight, serum, and urine biochemistries in CTL and CKD mice.

Parameters	CTL (n = 12)	CKD (n = 8)	*P* Value
Body Weight (g)	27.07 ± 1.81	19.06 ± 2.75	<0.0001
Serum			
BUN (mg/dL)	25.51 ± 1.18	65.16 ± 1.82	<0.0001
Cr (mg/dL)	0.33 ± 0.00	0.58 ± 0.01	<0.0001
Ca (mg/dL)	9.70 ± 0.15	10.65 ± 0.18	<0.0001
Pi (mg/dL)	9.02 ± 0.24	13.32 ± 0.62	<0.0001
ALP (IU/L)	162.92 ± 22.06	120.80 ± 6.01	NS
PTH (pg/mL)	1070.35 ± 154.40	1967.13 ± 204.40	<0.01
FGF23 (ng/mL)	0.32 ± 0.05	47.74 ± 4.56	<0.0001
Total P1NP (ng/mL)	0.42 ± 0.08	0.78 ± 0.09	<0.01
αCTx (ng/mL)	6.19 ± 1.86	16.45 ± 1.97	<0.01
Urine			
Cr (mg/dl)	262.50 ± 18.30	62.50 ± 8.18	<0.0001
Albumin	141.25 ± 8.75	42.50 ± 8.18	<0.0001
SG	>1.04 ± 0.00	1.02 ± 0.00	<0.0001
Urine/Serum ratio			
UCr/SCr	799.93 ± 49.51	99.72 ± 11.58	<0.0001

BUN, blood urea nitrogen; Cr, creatinine; Ca, calcium; Pi, phosphorus; ALP, alkaline phosphatase; PTH, parathyroid hormone; FGF23, fibroblast growth factor 23; SG, specific gravity; UACR, urine albumin/urine creatinine ratio; UCr/SCr, urine creatinine/serum creatinine. The data are represented as the means ± SEM.

Figure legends

Fig 1. Schematic view of the 5-week adenine induced CKD model and time-dependent changes in body weight. (A) Eight-week-old C57BL/6 male mice were randomly allocated to either a control (CTL; n=12) or CKD (n = 12) group. Mice in the CKD group were fed a casein-based diet containing 0.2% adenine diet for 5 weeks. Mice in the CTL group were fed a casein-based diet without adenine. (B) The bodyweight of the CKD mice progressively decreased during the 5-weeks on the adenine diet. The data are represented as the means ± SEM. **** $p < 0.0001$ as compared to CTL mice of the same age. Note, 4 mice in the CKD group lost more than 30% of their body weight and were removed from the study.

Fig 2. Micro-CT analysis of trabecular and cortical bone from CTL and CKD mice. Micro-CT analysis of tibia from mice fed a CTL or CKD diet for 5 weeks. (A) Quantification of Tb. BMD (trabecular bone mineral density), Tb. BV/TV (bone volume/tissue volume), Tb. Th (thickness), Tb. N (number), Tb. SMI (structural model index) (B) Cortical bone analyses

of Ct. BMD, Ct. BV/TV, Ct Th, Ct. CSA (cross-sectional area), and Ct Po (cl) (percent of porosity (close pores)) at 37% and 50% of the total tibial length from the top of the tibia. (C) Representative 3D micro-CT images of trabecular and cortical bone of CTL and CKD mice. The data are represented as the mean ± SEM (n = 8), * $p < 0.05$; *** $p < 0.001$; **** $p < 0.0001$.

Fig 3. Histological characterization of trabecular bone in CKD mice (A) Representative photomicrographs of tibia sections stained for hematoxylin and eosin (H&E; i & ii) and Goldner's trichrome (iii & iv) and reacted for tartrate acid phosphatase activity (TRAP; v & vi; blue arrow) from CTL and CKD mice at end of study (13 weeks of age). Scale bar, 100 μm. (B) Quantification of bone volume/tissue volume (BV/TV); osteoid volume/bone volume (OV/BV); osteoclast surface/bone surface (Oc.S/BS); number of osteoclasts/bone surface (N.Oc/BS); the data are represented as the mean ± SEM (n ≥ 6); * $p < 0.05$; ** $p < 0.01$.

Fig 4. Expression of osteoblast and mineralization markers in mouse femurs from CTL and CKD mice. (A) *E*xpression of key mineralization and osteoblast marker genes in femurs of CTL and CKD mice at end of the study (13 weeks of age). (B) Representative image of 2 CTL and 2 CKD femurs analyzed by western blot for PHOSPHO1 and TNAP expression (C) Quantification of PHOSPHO1 and TNAP expression in the femur of CTL and CKD mice. The data are represented as the mean ± SEM (n ≥ 8); * $p < 0.05$; ** $p < 0.01$; *** $p < 0.001$; **** $p < 0.0001$).

Fig 5. Micro-CT analysis of cortical bone of wild-type and PHOSPHO1 deficient CTL and CKD mice. Quantification of cortical bone mineral density (Ct. BMD), cortical bone volume/tissue volume (Ct. BV/TV), cortical cross-sectional area (Ct. CSA), cortical thickness (Ct. Th), and closed pore porosity (Ct Po (cl)) at 50% of the total tibial length from the top of the tibia. The data are represented as the mean ± SEM (n = 8); * $p < 0.05$; ** $p < 0.001$; **** $p < 0.0001$.

Fig 6. Regulation of key mineralization associated genes by Pi, PTH and FGF23 in primary osteoblasts. Expression analysis of *Phospho1, Alpl, Enpp1, Spp1, Slc20a1, Slc20a2, Bglap, and Runx2* by osteoblasts in response to (A) Pi (1-5 mM), (B) PTH (0-50 nM), and (C) FGF23 (0-200 ng/ml) for 28 days after confluency. The data are represented as the mean ± SEM (n = 3); *$p < 0.05$; ** $p < 0.01$; *** $p < 0.001$; **** $p < 0.0001$.

Fig 7. Regulation of key mineralization-associated proteins by Pi, PTH, and FGF23 in primary osteoblasts. Western blotting analysis and quantification of PHOSPHO1 and TNAP expression in response to (A) Pi (1-5 mM), (B) PTH (0-50 nM), and (C) FGF23 (0-200 ng/ml) for 28 days after confluency. The data are represented as the mean ± SEM (n = 3); * $p < 0.05$; ** $p < 0.01$; *** $p < 0.001$; **** $p < 0.0001$.

Fig 8. Regulation of osteoblast extracellular matrix mineralization by Pi, PTH, and FGF23. Representative images and quantification of alizarin red staining in response to (A) Pi (1-5 mM), (B) PTH (0-50 nM), and (C) FGF23 (0-200 ng/ml) for 28 days after confluency. The data are represented as the mean ± SEM (n = 3); *** $p < 0.001$; **** $p < 0.0001$.

Supplementary figure legends

Fig S1. Characterization of renal pathology in CKD mouse model. (A) Representative photomicrographs of hematoxylin and eosin (H&E; i-iv), Masson's trichrome (MT; v & vi), and von Kossa (VK; vii & viii) stained kidney sections from CTL and CKD mice at end of the study (13 weeks of age). (i & ii) kidney sections showing gross pathology, (d) atrophic tubuli with protein casts (green arrows) and dilated Bowman's space (blue arrow). (f) Dilated tubules (green arrows) and interstitial fibrosis (blue arrows. (h) Calcification of tubular structures (blue arrows). Scale bar, (i & ii) 500 μm, (iii-viii) 100 μm. (B) Renal scoring of tubular atrophy, protein casts, interstitial inflammation, and renal fibrosis of sections from 4 CTL and 4 CKD mice. Renal scoring scale: 0 = normal; 1 = mild, involvement of <25% of the cortex; 2 = moderate, involvement of 25 to 50% of the cortex; 3 = severe, involvement of 50 to 75% of the cortex; 4 = extensive damage involving >75% of the cortex. The data are represented as the mean ± SEM (n = 4); **** $p < 0.0001$.

Fig S2. Expression levels of kidney injury associated markers in CTL and CKD mice. (A) *Fgf23, Slc34a1, Spp1, and Lcn2* expression in kidneys of CTL and CKD mice at end of the study (13 weeks of age). Four random samples from each of the CTL and CKD groups were selected for analysis. (B) Representative western blot of osteopontin (OPN) and type II sodium-phosphate cotransporter (NaPi-2a) protein expression from BBMV of kidneys at end of study (13 weeks of age).

Fig S3. Characterization of osteoblast culture model showing temporal increases in extracellular matrix mineralization and PHOSPHO1 and TNAP expression. (A) Alizarin red staining, (B) quantification of matrix mineralization (C) RT-qPCR analysis of *Phospho1*, and *Alpl* mRNA expression, (D) western blot analysis, and (E) quantification of PHOSPHO1, and TNAP expression and by primary osteoblasts cultured in the basal Pi-substrate free mineralization medium over a 28-day culture period. The data are represented as the mean ± SEM (n = 3); * $p < 0.05$; ** $p < 0.01$; *** $p < 0.001$; **** $p < 0.0001$ in comparison with day 0, post confluence cultures.

Fig S4. The effect of Pi on osteoblast viability. Cells were exposed to Pi (1-5 mM) for 28 days after confluency and viability were assessed by (A) Alamar Blue assay, and (B) LDH assay. The data are represented as the mean ± SEM (n = 4); NS, not significance from the 1 mM control group.

Fig S5 Regulation of key mineralization associated genes by FGF23 + klotho by primary osteoblasts. Expression analysis of *Phospho1, Alpl, Enpp1, Spp1, Slc20a1, Slc20a2, Bglap, and Runx2* by osteoblasts in response to FGF23 (F) (0 - 200 ng/ml) + klotho (KL) (50ng/ml) for 28 days after confluency. The data are represented as the mean ± SEM (n = 3); NS not significant, ** $p < 0.01$; *** $p < 0.001$.

Fig S6. Regulation of key mineralization-associated proteins and Alizarin red staining by FGF23 + klotho by primary osteoblasts. (A) Western blotting analysis and (B) quantification of PHOSPHO1 and TNAP expression in response to FGF23 (F) (0-200 ng/ml) + klotho (KL) (50ng/ml) for 28 days after confluency. (C & D) Representative images of Alizarin red staining and quantification of matrix mineralization. The data are represented as the mean ± SEM (n = 3); NS, not significant, ** $p < 0.01$.

Supplementary tables

Table S1. Sequences of primers used for qPCR

Genes	Forward, 5'→ 3'	Reverse, 5'→ 3'	Source
Atp5b	ATGCCACTTCCAAGGTAGCG	GCAACAGTCAGACCAGTCAGA	Primer Design
Gapdh	AAATGGTGAAGGTCGGTGTG	TGAAGGGGTCGTTGATGG	Sigma-Aldrich
Phospho1	TTCTCATTTCGGATGCCAACA	TGAGGATGCGGCGGAATAA	Eurofins Genomics
Alpl	GGGACGAATCTCAGGGTACA	AGTAACTGGGGTCTCTCTC	Sigma-Aldrich
Enpp1	GCTAATCATCAGGAGGTCAAG	CTGGTAGAATCCCGTCAATC	Sigma-Aldrich
Spp1	CACTCCAATCGTCCCTACAGT	CTGGAAACTCCTAGACTTTGACC	Sigma-Aldrich
Slc20a1	TGTGGCAAATGGGCAGAAG	AGAAAGCAGCGGAGAGACGA	Sigma-Aldrich
Slc20a2	CCATCGGCTTCTCACTCGT	AAACCAGGAGGCGACAATCT	Sigma-Aldrich
Anxa6	GGACCTCATCGAAGACTTGAAG	CTTTGGCGTCACAATAGGCAA	Sigma-Aldrich
Ank	TCGCTGCCTTCCCTTTTATG	GGTGACTGTGAAGCAAAATGG	Sigma-Aldrich
Npnt	TGCCCTATCGTGTTCCATG	ACTCTTCCAGTCGCACATTC	Sigma-Aldrich
Pdpn	AACAAGTCACCCCAATAGAGATAAT	CTAACAAGACGCCAACTATGATTC	Sigma-Aldrich
Fgf23	GGATCTCCACGGCAACATTT	GTAGTGATGCTTCTGCGACAA	Eurofins Genomics
Bglap	CCGGGAGCAGTGTGAGCTTA	TAGATGCGTTTGTAGGCGGTC	Sigma-Aldrich
Runx2	ACCATAACAGTCTTCACAAATCCT	CAGGCGATCAGAGAACAAACTA	Sigma-Aldrich
Sost	TGAGAACAACCAGACCATGAAC	TCAGGAAGCGGGTGTAGTG	Primer Design
Bmp2	TCAAGCCAAACACAAACAGC	AGCCACAATCCAGTCATTCC	Sigma-Aldrich
Klotho	GGACAATGGCTTTCCTCCTT	TGCACATCCCACAGATAGACA	Sigma-Aldrich
Adipoq	AAGAAGGACAAGGCCGTTCTCTT	GCTATGGGTAGTTGCAGTCAGTT	Sigma-Aldrich

Table S2. Primary antibodies used for western blotting

Target	Source	Company	Dilution	Molecular weight
β-actin	Rabbit	Cell Signaling Technology	1:4000	45 kDa
PHOSPHO1	Human	AbD Serotec and Bio-Rad	1:500	32 kDa
TNAP	Rat	R&D Systems	1:1000	75 kDa

Table S3. Secondary antibodies used for western blotting

Target	Source	Company	Dilution
β-actin	Goat anti-rabbit	Dako	1:1000
PHOSPHO1	Goat anti-human	Bio-Rad	1:1000
TNAP	Goat anti-rat	R&D Systems	1:1000
β-actin	Donkey anti-rabbit	LI-COR Biosciences	1:15000
PHOSPHO1	Goat anti-human	LI-COR Biosciences	1:15000
TNAP	Goat anti-rat	LI-COR Biosciences	1:15000

A

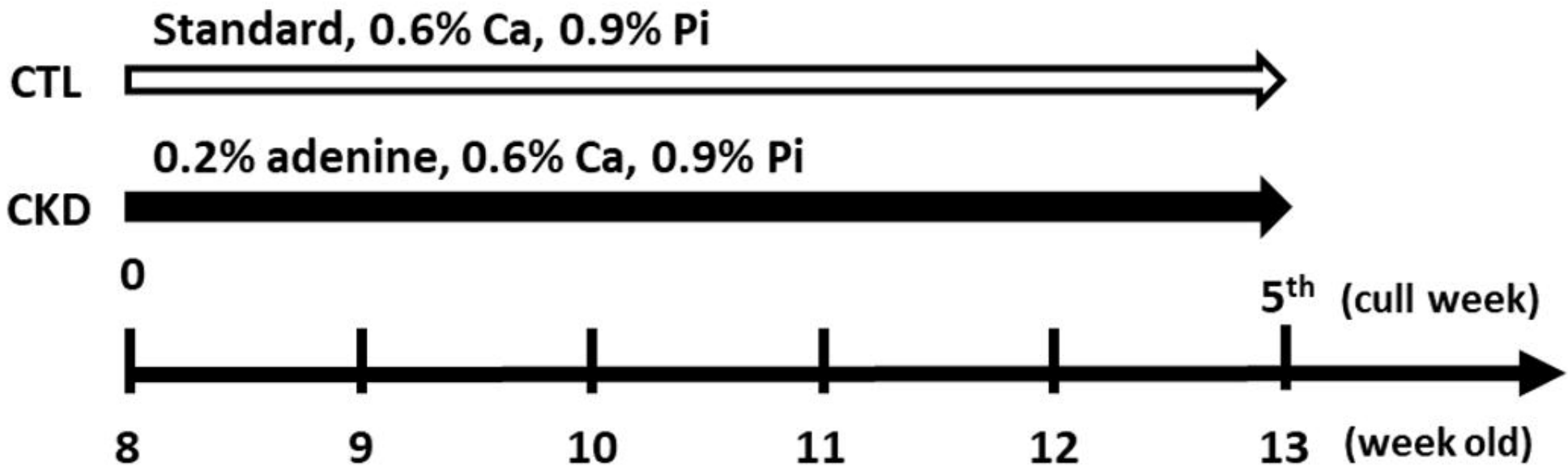
Standard, 0.6% Ca, 0.9% Pi
CTL
0.2% adenine, 0.6% Ca, 0.9% Pi
CKD
0
5th (cull week)
8
9
10
11
12
13
(week old)

B

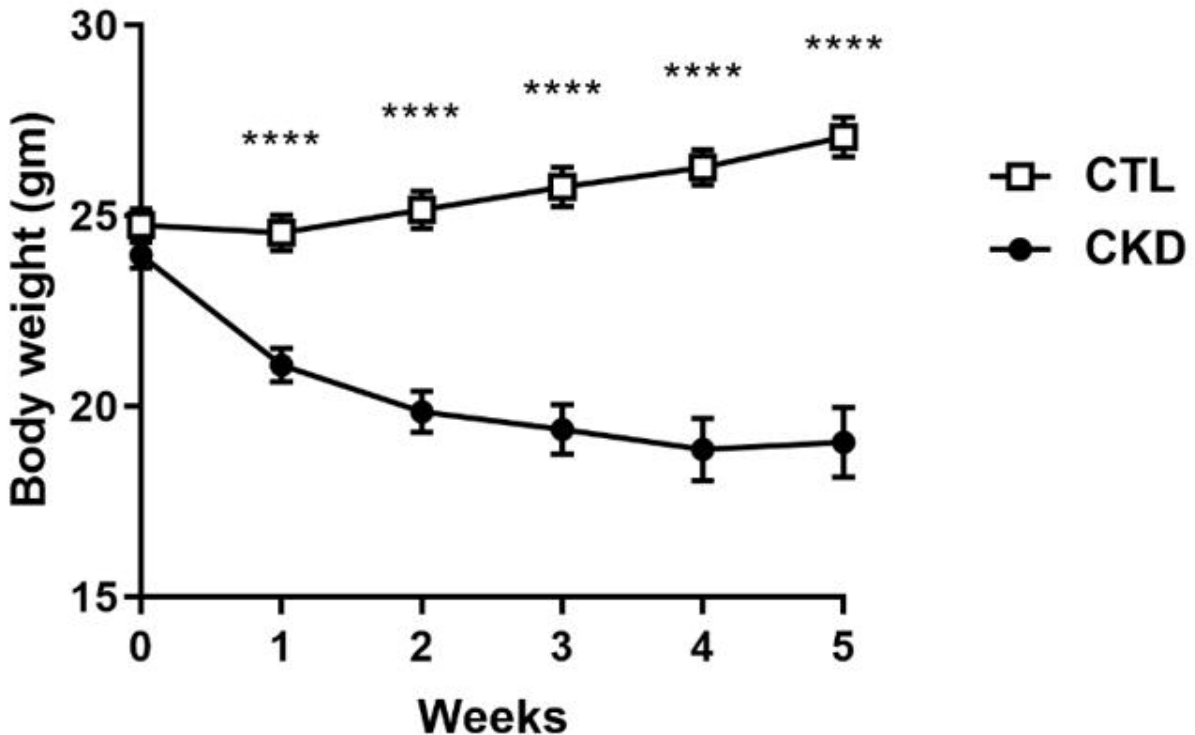
Body weight (gm)
30
25
20
15
0
1
2
3
4
5
Weeks
****
****
****
****
****
CTL
CKD

A

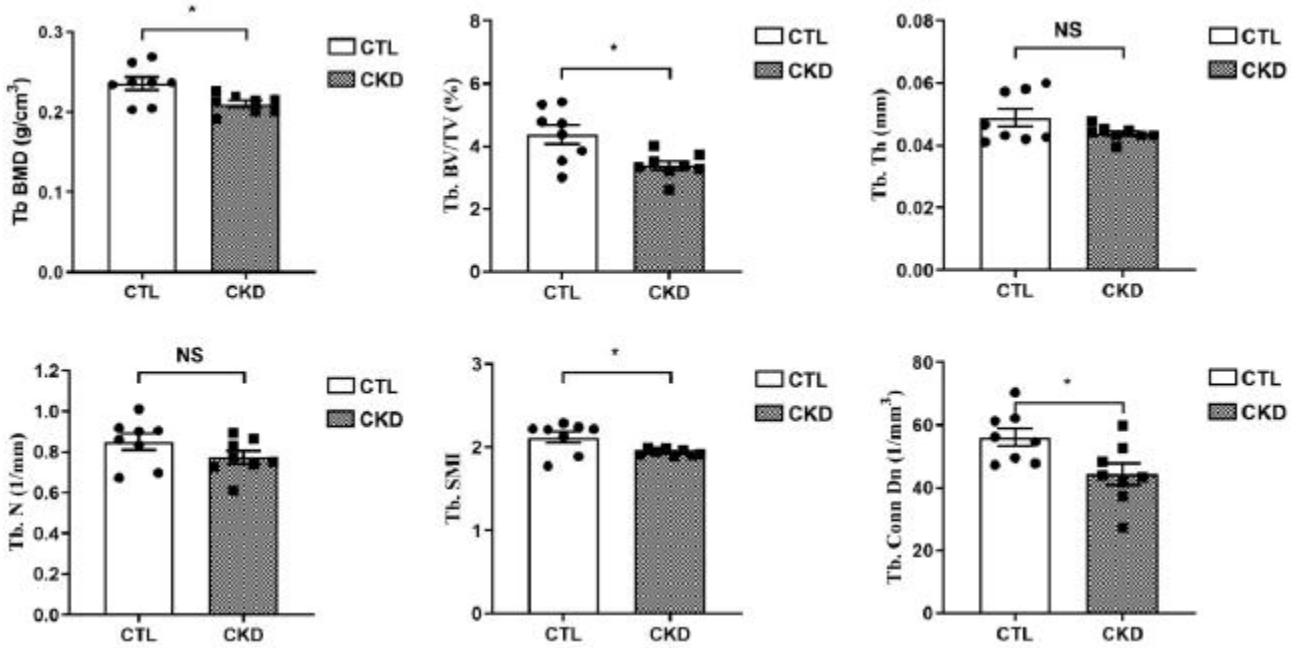
Tb BMD (g/cm³)
Tb. BV/TV (%)
Tb. Th (mm)
Tb. N (1/mm)
Tb. SMI
Tb. Conn Dn (1/mm³)
CTL
CKD
NS
*

B

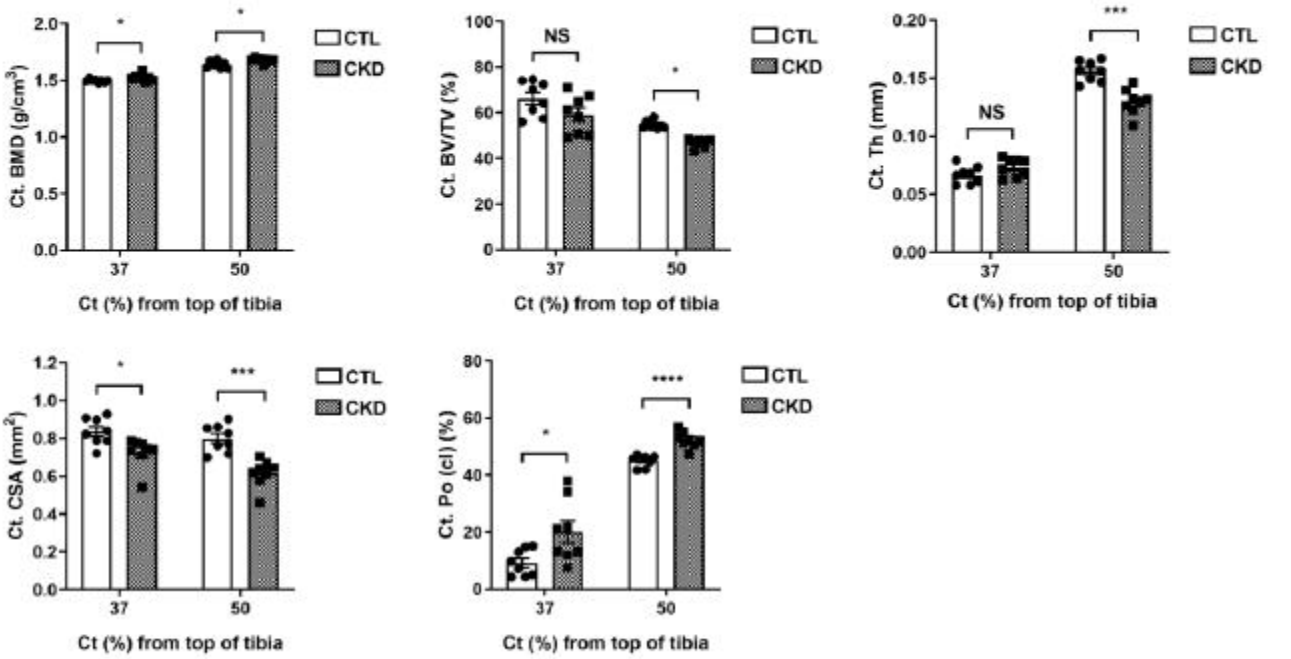
Ct. BMD (g/cm³)
Ct. BV/TV (%)
Ct. Th (mm)
Ct. CSA (mm²)
Ct. Po (cl) (%)
Ct (%) from top of tibia
37
50
CTL
CKD
NS
*
***
****

C

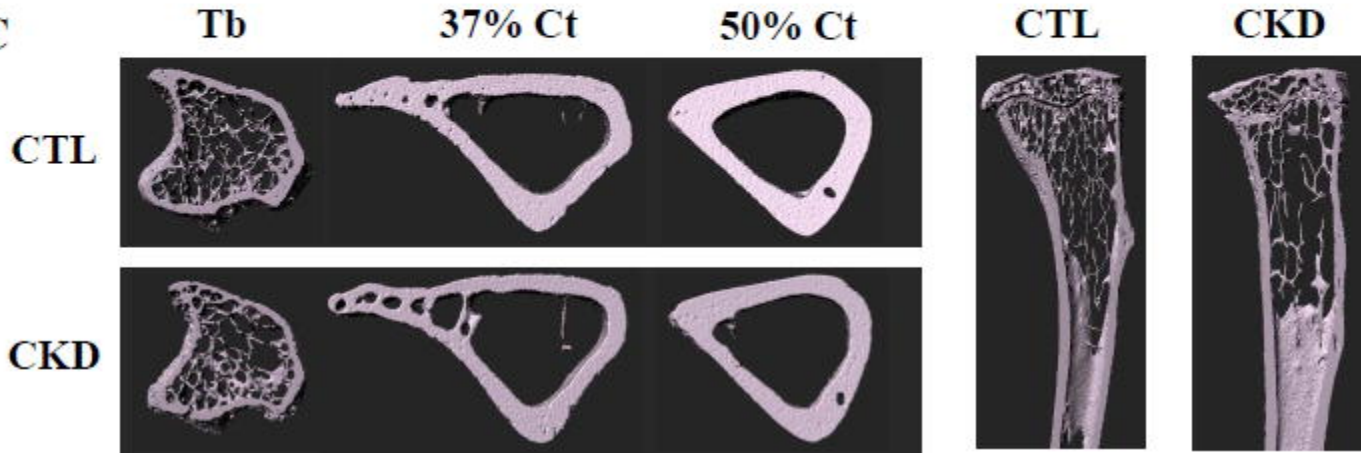
Tb
37% Ct
50% Ct
CTL
CKD

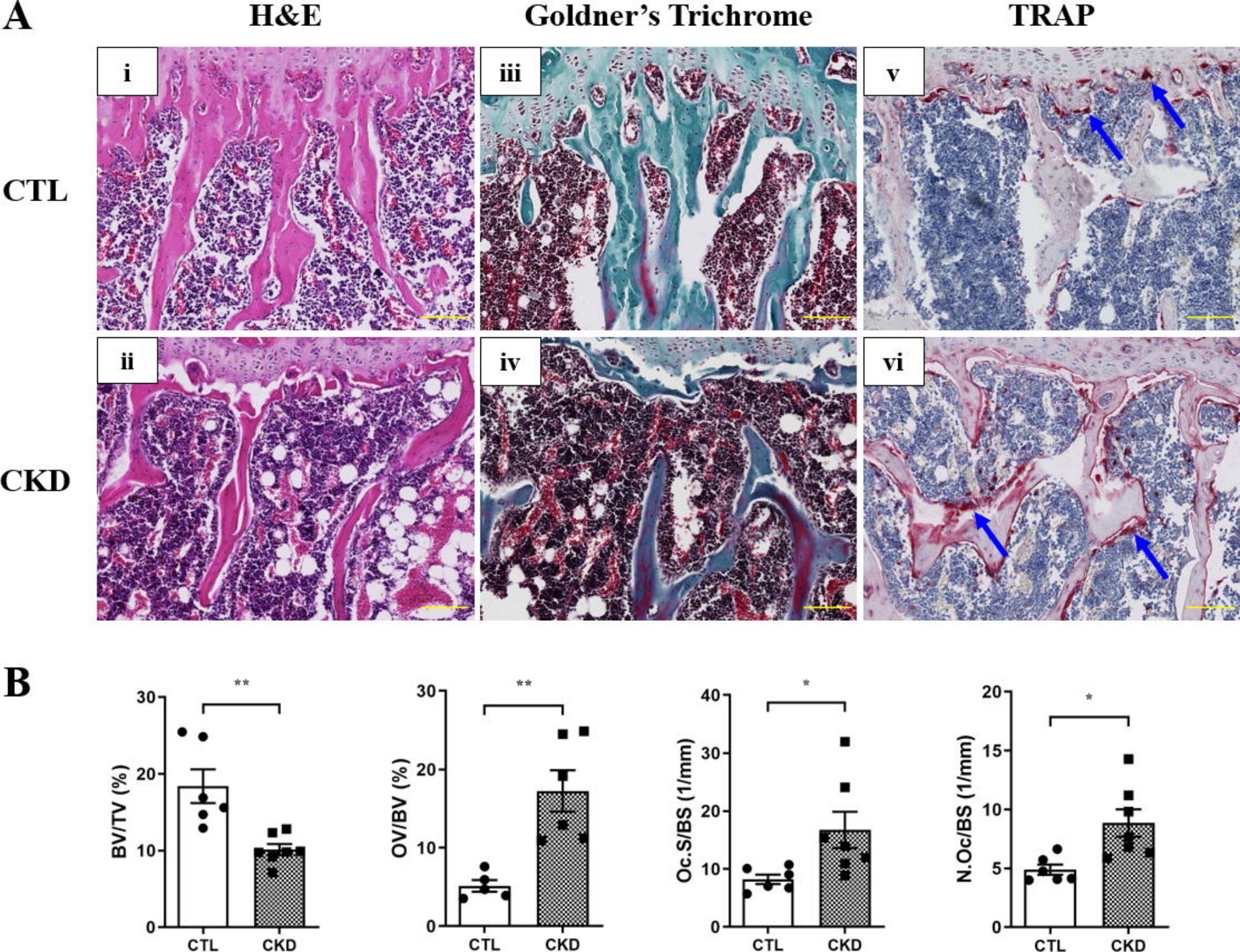
A
H&E
Goldner's Trichrome
TRAP
CTL
CKD
i
ii
iii
iv
v
vi
B
BV/TV (%)
OV/BV (%)
Oc.S/BS (1/mm)
N.Oc/BS (1/mm)
CTL
CKD
**
*

A

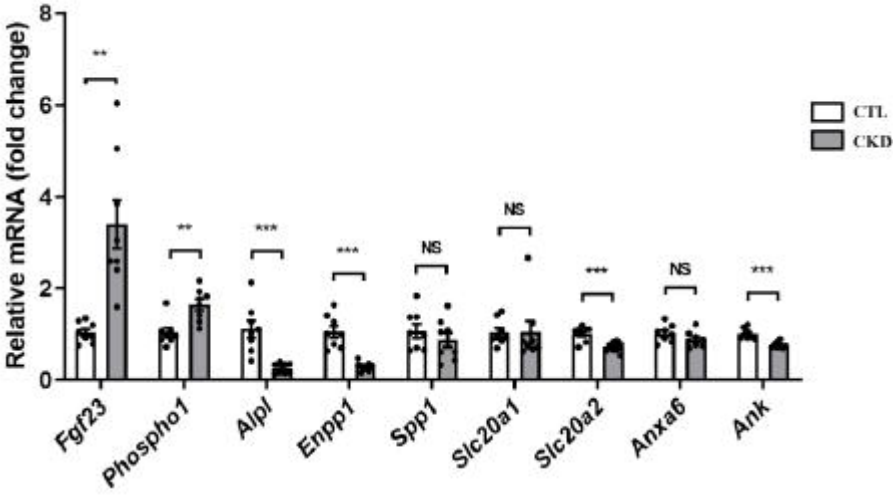
Relative mRNA (fold change)
CTL
CKD
Fgf23
Phospho1
Alpl
Enpp1
Spp1
Slc20a1
Slc20a2
Anxa6
Ank

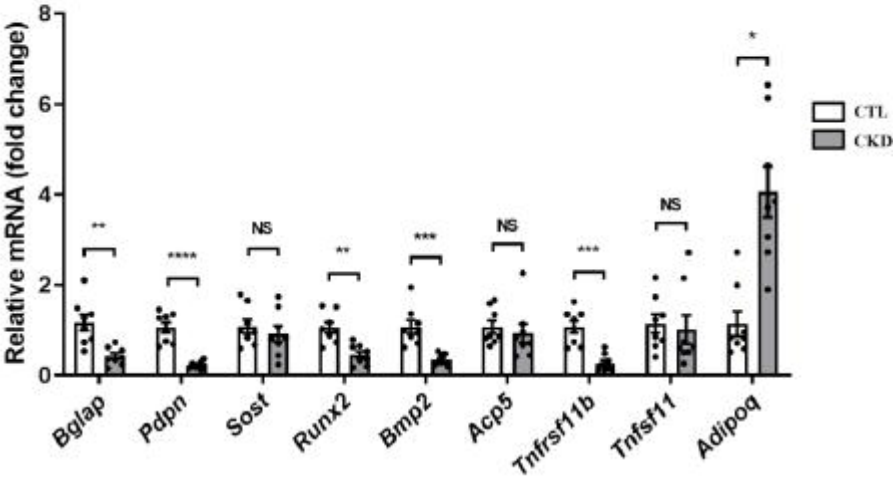
Relative mRNA (fold change)
CTL
CKD
Bglap
Pdpn
Sost
Runx2
Bmp2
Acp5
Tnfrsf11b
Tnfsf11
Adipoq

B

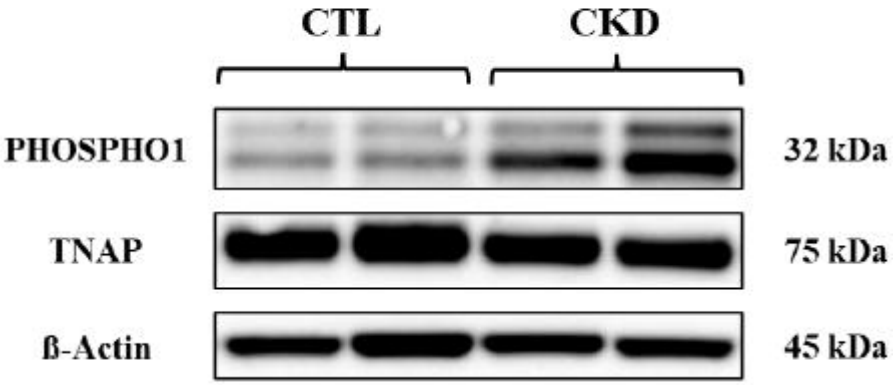
CTL
CKD
PHOSPHO1
32 kDa
TNAP
75 kDa
ß-Actin
45 kDa

C

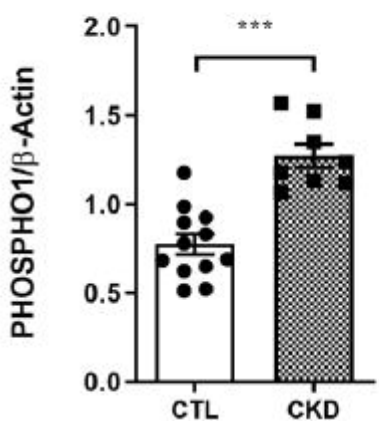
PHOSPHO1/β-Actin
CTL
CKD

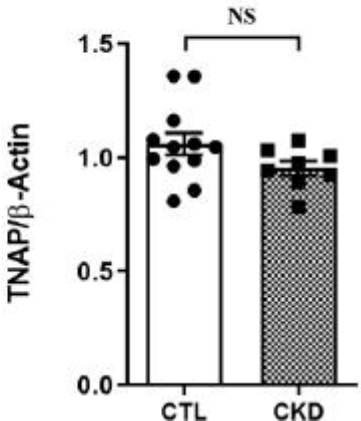
TNAP/β-Actin
NS
CTL
CKD

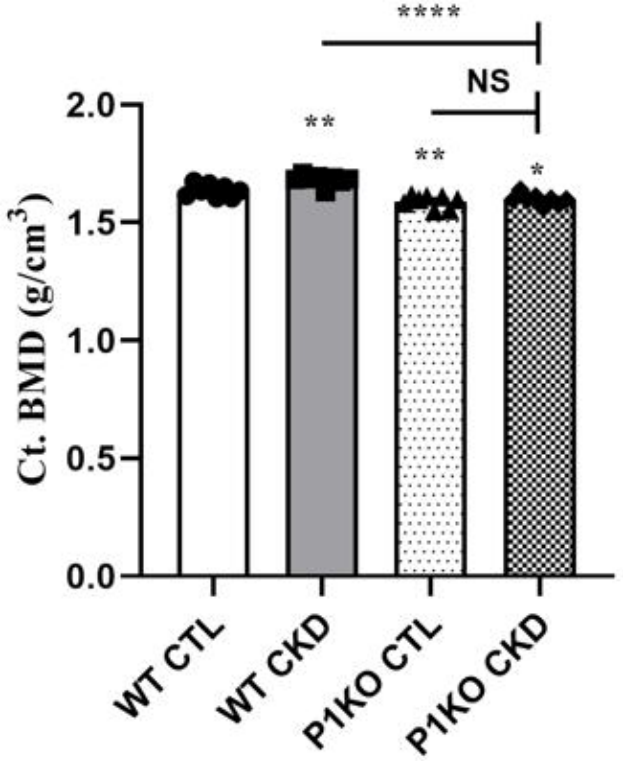
****
NS
**
**
*
Ct. BMD (g/cm3)
2.0
1.5
1.0
0.5
0.0
WT CTL
WT CKD
P1KO CTL
P1KO CKD

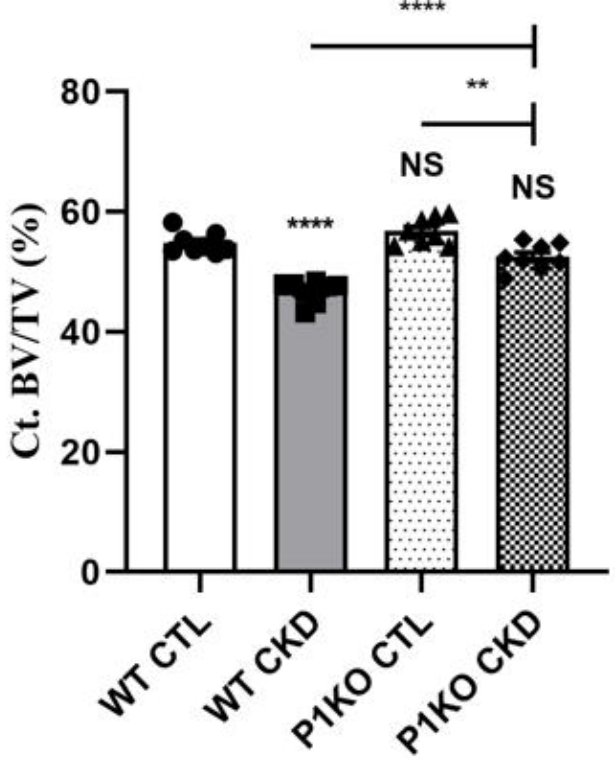
****
**
NS
NS
****
Ct. BV/TV (%)
80
60
40
20
0
WT CTL
WT CKD
P1KO CTL
P1KO CKD

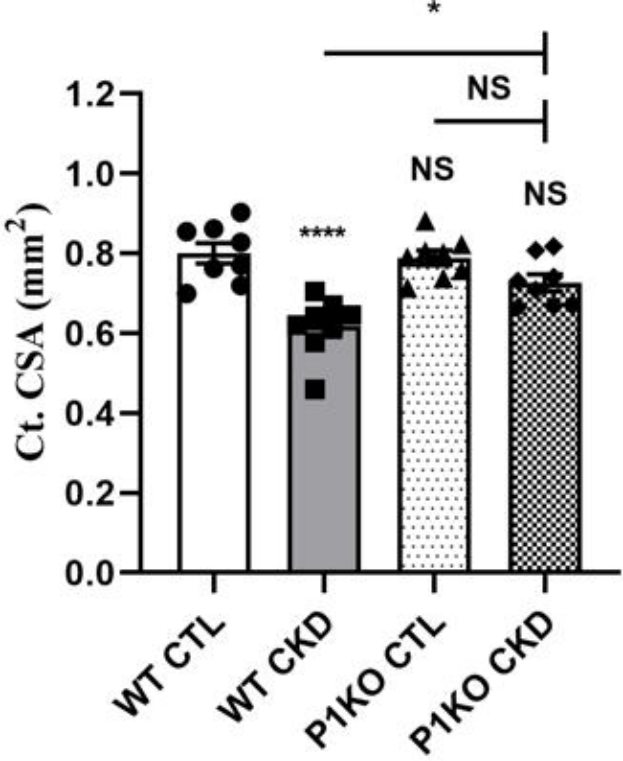
*
NS
NS
NS
****
Ct. CSA (mm2)
1.2
1.0
0.8
0.6
0.4
0.2
0.0
WT CTL
WT CKD
P1KO CTL
P1KO CKD

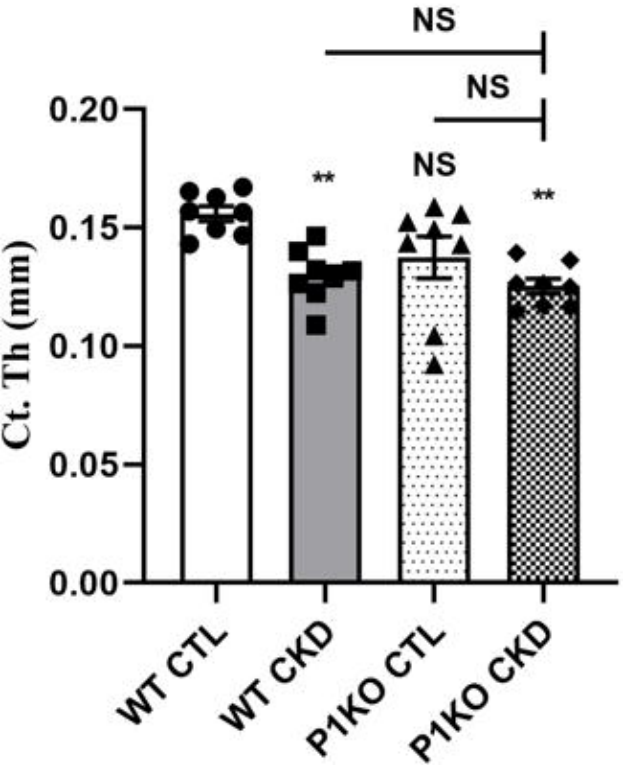
NS
NS
NS
**
**
Ct. Th (mm)
0.20
0.15
0.10
0.05
0.00
WT CTL
WT CKD
P1KO CTL
P1KO CKD

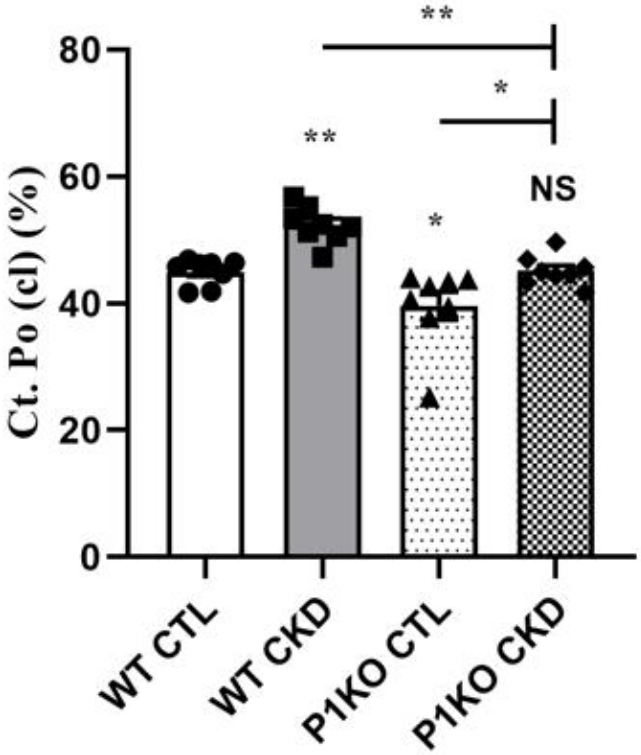
**
*
**
*
NS
Ct. Po (cl) (%)
80
60
40
20
0
WT CTL
WT CKD
P1KO CTL
P1KO CKD

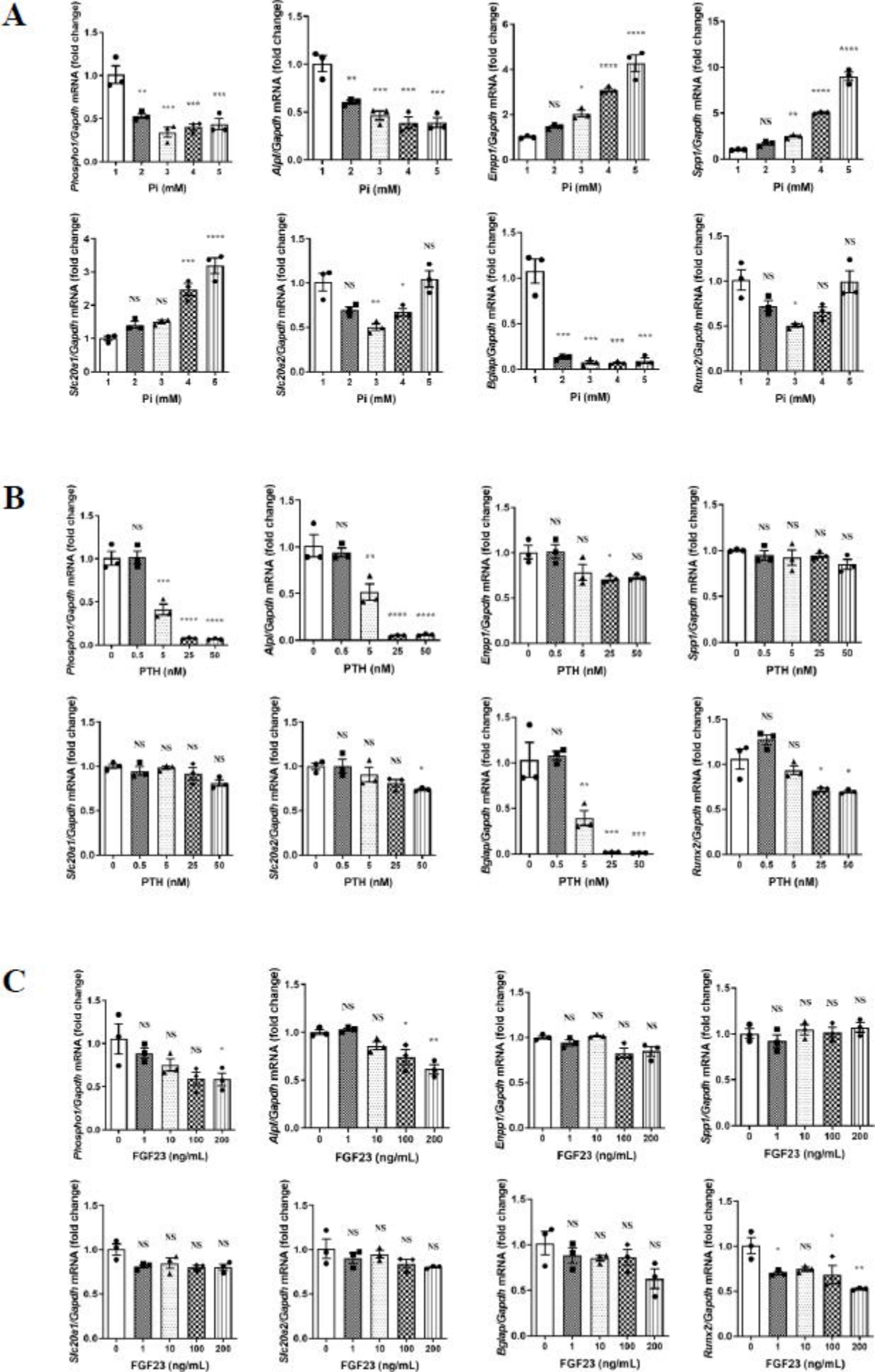
A
Phospho1/Gapdh mRNA (fold change)
Alpl/Gapdh mRNA (fold change)
Enpp1/Gapdh mRNA (fold change)
Spp1/Gapdh mRNA (fold change)
Slc20a1/Gapdh mRNA (fold change)
Slc20a2/Gapdh mRNA (fold change)
Bglap/Gapdh mRNA (fold change)
Runx2/Gapdh mRNA (fold change)
Pi (mM)
B
PTH (nM)
C
FGF23 (ng/mL)

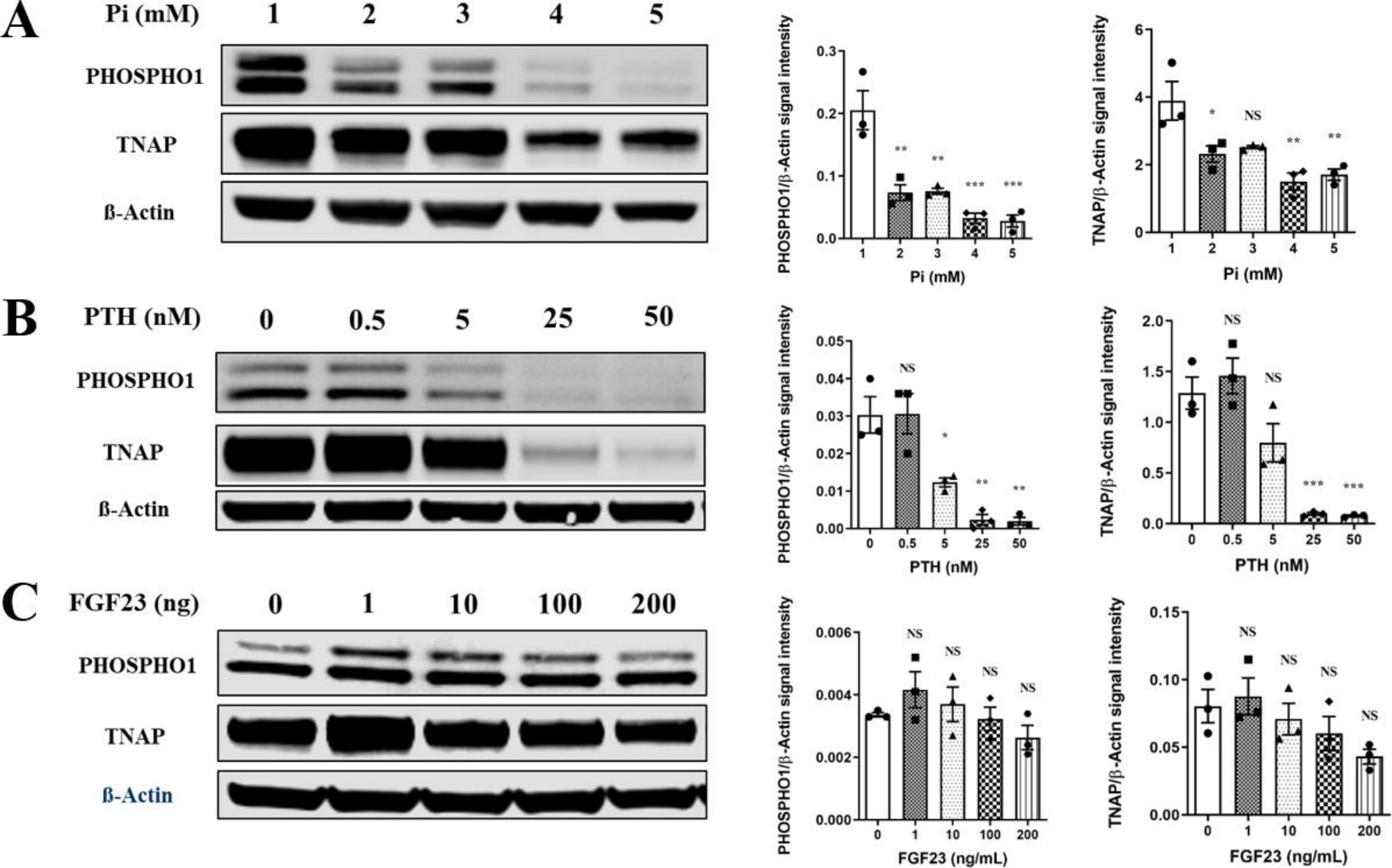
A
Pi (mM)
1
2
3
4
5
PHOSPHO1
TNAP
ß-Actin
PHOSPHO1/β-Actin signal intensity
Pi (mM)
TNAP/β-Actin signal intensity
Pi (mM)
B
PTH (nM)
0
0.5
5
25
50
PHOSPHO1
TNAP
ß-Actin
PHOSPHO1/β-Actin signal intensity
PTH (nM)
TNAP/β-Actin signal intensity
PTH (nM)
C
FGF23 (ng)
0
1
10
100
200
PHOSPHO1
TNAP
ß-Actin
PHOSPHO1/β-Actin signal intensity
FGF23 (ng/mL)
TNAP/β-Actin signal intensity
FGF23 (ng/mL)

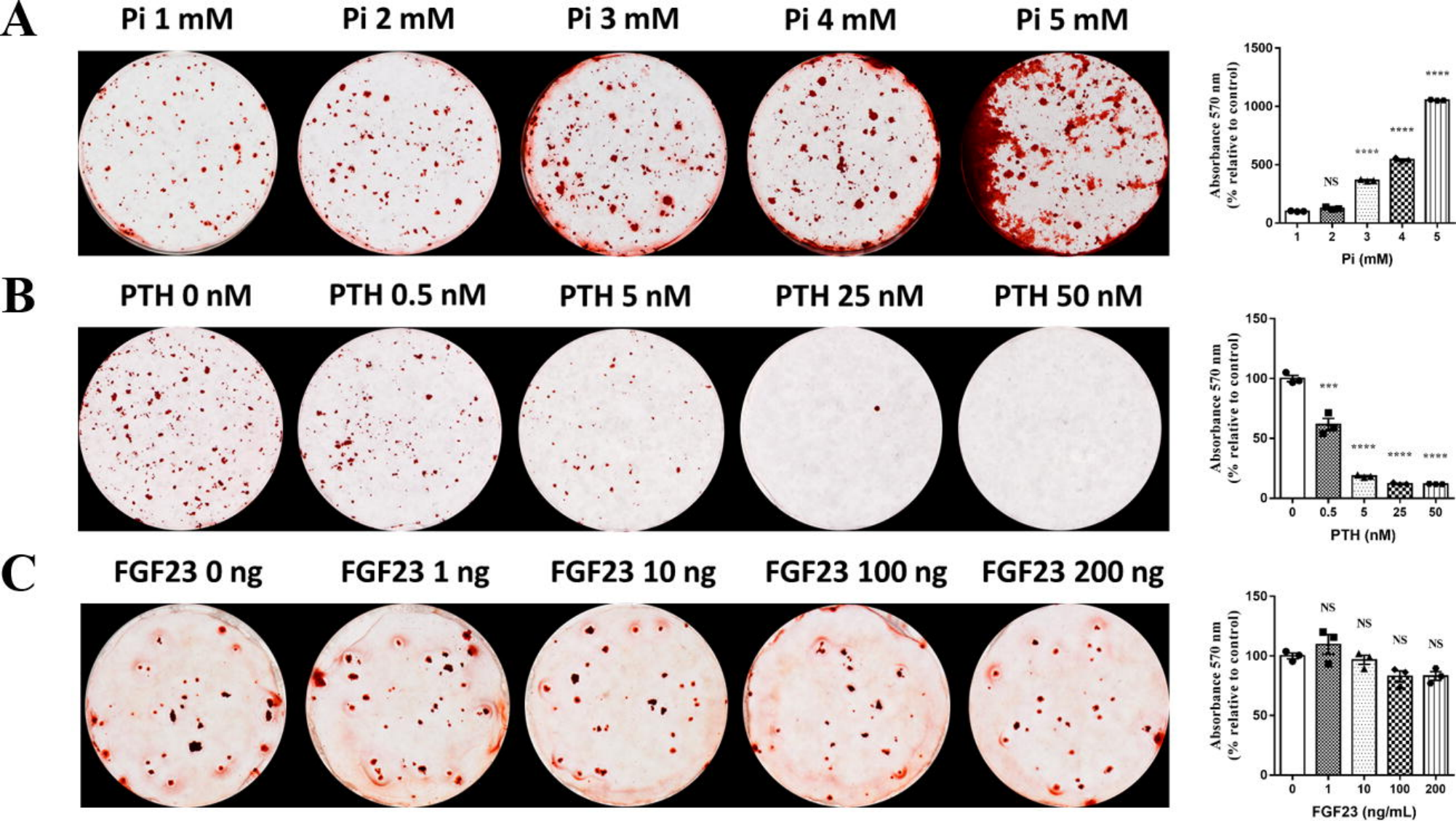
A
Pi 1 mM
Pi 2 mM
Pi 3 mM
Pi 4 mM
Pi 5 mM
Absorbance 570 nm (% relative to control)
1500
1000
500
0
NS
****
****
****
1
2
3
4
5
Pi (mM)
B
PTH 0 nM
PTH 0.5 nM
PTH 5 nM
PTH 25 nM
PTH 50 nM
Absorbance 570 nm (% relative to control)
150
100
50
0
***
****
****
****
0
0.5
5
25
50
PTH (nM)
C
FGF23 0 ng
FGF23 1 ng
FGF23 10 ng
FGF23 100 ng
FGF23 200 ng
Absorbance 570 nm (% relative to control)
150
100
50
0
NS
NS
NS
NS
0
1
10
100
200
FGF23 (ng/mL)